INFORMATION TO USERS

This manuscript has been reproduced from the microfilm master. UMI films the text directly from the original or copy submitted. Thus, some thesis and dissertation copies are in typewriter face, while others may be from any type of computer printer.

The quality of this reproduction is dependent upon the quality of the copy submitted. Broken or indistinct print, colored or poor quality illustrations and photographs, print bleedthrough, substandard margins, and improper alignment can adversely affect reproduction.

In the unlikely event that the author did not send UMI a complete manuscript and there are missing pages, these will be noted. Also, if unauthorized copyright material had to be removed, a note will indicate the deletion.

Oversize materials (e.g., maps, drawings, charts) are reproduced by sectioning the original, beginning at the upper left-hand corner and continuing from left to right in equal sections with small overlaps.

Photographs included in the original manuscript have been reproduced xerographically in this copy. Higher quality 6" x 9" black and white photographic prints are available for any photographs or illustrations appearing in this copy for an additional charge. Contact UMI directly to order.

Bell & Howell Information and Learning
300 North Zeeb Road, Ann Arbor, MI 48106-1346 USA
800-521-0600

Circumferential propagation of acoustic pulses in partially-filled cylindrical shells

Kevin Shannon

A Thesis

in

The Department

of

Physics

Presented in Partial Fulfillment of the Requirements
for the Degree of Master of Science at
Concordia University
Montreal, Quebec, Canada

June 2000

© Kevin Shannon, 2000

National Library of Canada
Acquisitions and Bibliographic Services
395 Wellington Street
Ottawa ON K1A 0N4
Canada

Bibliothèque nationale du Canada
Acquisitions et services bibliographiques
395, rue Wellington
Ottawa ON K1A 0N4
Canada

Your file Votre référence

Our file Notre référence

The author has granted a non-exclusive licence allowing the National Library of Canada to reproduce, loan, distribute or sell copies of this thesis in microform, paper or electronic formats.

L'auteur a accordé une licence non exclusive permettant à la Bibliothèque nationale du Canada de reproduire, prêter, distribuer ou vendre des copies de cette thèse sous la forme de microfiche/film, de reproduction sur papier ou sur format électronique.

The author retains ownership of the copyright in this thesis. Neither the thesis nor substantial extracts from it may be printed or otherwise reproduced without the author's permission.

L'auteur conserve la propriété du droit d'auteur qui protège cette thèse. Ni la thèse ni des extraits substantiels de celle-ci ne doivent être imprimés ou autrement reproduits sans son autorisation.

0-612-54298-X

Canada

ABSTRACT

Circumferential propagation of acoustic pulses in partially-filled cylindrical shells

Kevin Shannon

We investigate the circumferential propagation of acoustic pulses in partially water-filled aluminum and stainless steel thin-walled cylindrical shells in the frequency x thickness (fd) region 0.64 MHz mm < fd < 0.96 MHz mm. In pulse-echo experiments, a multiplicity of periodic echoes were received when a single input pulse was applied to the outer surface of the shell. The periodic behaviour suggests that the pulses take different paths within the system, and that these paths depend upon the height of the liquid filler. Computer simulation and obstruction experiments are used to determine the nature of these paths, and identify, in particular, which modes propagate within the water-loaded portions of the shells. This work suggests that the A_0 Lamb-like wave predominates in the loaded shell. The application to liquid-level sensing is investigated.

ACKNOWLEDGEMENT AND DEDICATION

Though there is one name on the cover of this thesis, its contents are borne of many peoples' effort. The greatest contribution, of course, comes through Dr. Cheeke's his years of guidance and supervision. Similarly, professor Z. Wang and Xing Li have contributed much in technical guidance over my years at Concordia.

I would like to thank my friends and fellow students Manas, Julien, Gino, Yuxing, Gurnam and Mario variously for hours at the blackboard, and offers of coffee. You knew not what encouragement lay in those simple gestures. Gloria, Lynn and Moustaffa were equally effective in brightening my days spent in the lab.

I must thanks John Monaghan, my roommate, for letting the dishes slide one more time as his friend turned a cold shoulder to conversation in favor of his simulation. Thanks, again, John.

This work is dedicated to my mother, Winnie. Without her dedication to education, and her persistent enthusiasm and support, this work would not have been possible.

Thank you all. Your lessons are not lost.

Kevin Shannon

Table of Contents

List of Figures

List of Tables

1. INTRODUCTION

In 1994, the Concordia University Sensor Group undertook research on circumferential modes in fluid-loaded structures. The research was motivated by the suggestion that circumferential waves could perhaps be used as a non-intrusive means of detecting liquid levels inside pipes and tubing. Such a detection technique has been researched and reported upon for level detection in upright cylinders and tanks [1]. Few results have been published, however, on the use of circumferential waves for level detection in cylindrical shells with a horizontal main axis.

A novel method of generating circumferential waves was developed at Concordia [2 - 4]. The approach used an interdigital transducer (IDT) permanently coupled to the shell's outer surface to generate and receive the circumferential acoustic pulses. This technique effectively generated coupled modes in the fully-filled stainless steel shell as predicted by Veksler *et al* [5] and Maze [6]. The close match between theory and experiment is reported in the recent doctoral dissertation by X. Li [7].

While the shell mounted IDT is a brilliant bit of technology, its application is limited to shells of small radius. It was found that, alternately, a common longitudinal bulk transducer could produce and receive the desired circumferential modes if it were coupled to the tube in a particular manner. This bulk transducer method is much less difficult to setup, and is more suited to field application.

When the bulk transducer produced a single pulse on a shell that was partially filled with liquid, multiple echoes were observed. The waveforms acquired at different liquid-levels exhibited different patterns of echoes. Each level, in effect, had a unique or

"signature" echo pattern. The obvious problem was to determine what causes this multiplicity of echoes. The implication is that perhaps this pattern might be used to determine the liquid level inside the shell.

To determine the liquid level using circumferential waves, we would need to have some prior idea of the echo pattern associated with each level for any liquid and shell tested. This could be accomplished using a neural network (NN) approach if there were the opportunity to train the NN on the shell beforehand. Such prior testing could well be impractical in many field applications. Alternately, we could endeavor to predict the echo pattern using our knowledge of acoustics and of the shell parameters.

This research presents the basis for the second approach. Specifically, we present the acoustic theory necessary to explain the echo patterns. We also test the theories for partially water-filled aluminum and stainless steel shells.

Because the acoustics of the system is not fully understood, especially when it comes to predicting which mode propagates along the portion of the shell that is coupled to the liquid, we must consider two competing theories, i.e. propagation of Lamb-like modes and propagation of "coupled modes"[1]. Lamb-like waves are surface waves that propagate along a thin plate loaded by liquid on one or both of its surfaces. Lamb-like modes can also be said to exist on slightly curved surfaces such as a circular shell made to vibrate at sufficiently high acoustic frequencies. Coupled modes, on the other hand, exist only in shells containing liquid, where there is coupling of acoustic modes in the shell and modes in the internal liquid [5].

Lamb-like modes are *leaky*, whereas coupled modes are not. As a result, the two types of modes take significantly different paths through the system, and cause very different echo patterns in the acquired waveform. In our efforts to understand the origin of the observed echo patterns, therefore, much attention will be given to a pulse's path through the system.

This document is divided into five chapters. Following this chapter is Chapter 2, "Theory", which establishes the acoustic theory needed to understand the echo patterns. Chapter 3, "Experiment", describes the experimental setup, techniques, and samples tested. Chapter 4, "Results and Analysis", isolates the time periods associated with each observed pattern, and compares these periods to theoretical flight times for various paths. In this way, we will endeavor to explain the observed patterns in terms of the modes in the system. Chapter 5, "Conclusion", highlights the main results of this research.

---

[1] In the absence of a standard nomenclature for these modes, we use the term "coupled" to refer to the modes identified in the literature variously as SWG [5] and WT [6].

2. THEORY

This chapter presents the acoustic principles for propagation of a pulse through the system. The system, shown in Figure 2.1, is a hollow cylindrical shell partially filled with liquid. We can distinguish four points in the system where unique phenomena occur:

(a) *Propagation in the unloaded portion of the cylinder.* We must know the group velocity, v_g, for the pulse here (section 2.1.1),

(b) *Action at an air-liquid interface* (section 2.1.5),

(c) *Propagation in the liquid-loaded portion of the cylinder.* We must know a pulse's group velocity, v_g^L, phase velocity, v_p^L, and attenuation. Because we do not know *a priori* which modes propagate around the liquid-loaded portion of the shell, we present the theory for the most likely candidates: the lowest order Lamb-like modes A_0^L and S_0^L, and the *coupled modes* described in section 2.2 (why these modes are most likely will be made clear later). We must also understand whether these modes leak into the liquid filler, and if so, then in which direction,

(d) *Bulk wave reflection and refraction at the cylinder wall* (section 2.1.4),

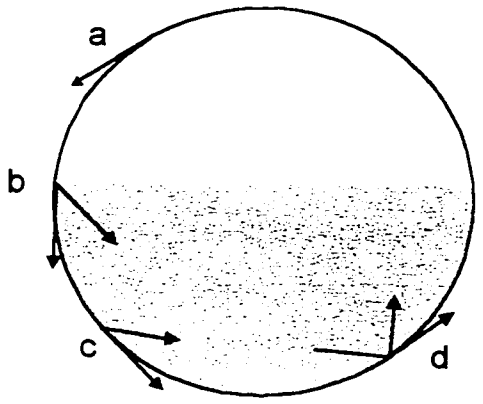

Figure 2.1

Physical phenomena described in this research

It has been the trend in the literature to compare the modes in fluid-loaded shells with those of a fluid-loaded plate. The close correspondence between the modes in the two systems is so well established that a single notation is usually used to refer to the modes in both systems [8 - 11]. The similarity is a fortunate one; we can use the simpler mathematics of the flat plate to derive the behavior of modes in the curved shell. This will be our method throughout this chapter: we will discuss the acoustics of the plate with the implication that the results are also true for the shell.

2.1 Plate modes

H. Lamb was first to report solutions to the wave equation describing the propagation of acoustic modes down an infinite plate in vacuum [12]. Osborne & Hart later applied Lamb's method to a plate immersed in a liquid [13]. Osborne & Hart's immersed modes were found to be analogous to the Lamb modes, except for the addition of an imaginary component to the wave vectors. Osborne & Hart referred to their immersed modes as "Lamb-like". Osborne & Hart also found an additional real solution to the wave equation. This real solution was shown to represent an evanescent wave propagating mostly in the liquid along the plate surface similar to the surface wave found by Stoneley. Grabowska extended the Osborne & Hart analysis to a plate separating a liquid from vacuum [14]. Talmant later solved the more general equation for Lamb-like modes in an infinite plate between two different liquids [15].

In the next section, we derive the equation for a wave travelling down an infinite plate under general loading conditions. The derivations are based on the work by Talmant [15]. The solutions to this equation provide us with valuable insight into the behavior of Lamb and Lamb-like modes.

2.1.1 Solutions to the wave equation

The general case of an infinite plate surrounded by two different liquids is shown in Figure 2.2. We shall use ρ_1, v_1, ρ_2, v_2 to denote the liquid density and sound velocity in liquids 1 and 2, respectively, and ρ, v_L, v_T to denote the density, longitudinal and transverse velocities in the plate. The system has continuity of pressure and particle displacement normal to the plate at both surfaces, $z = \pm e = \pm d/2$.

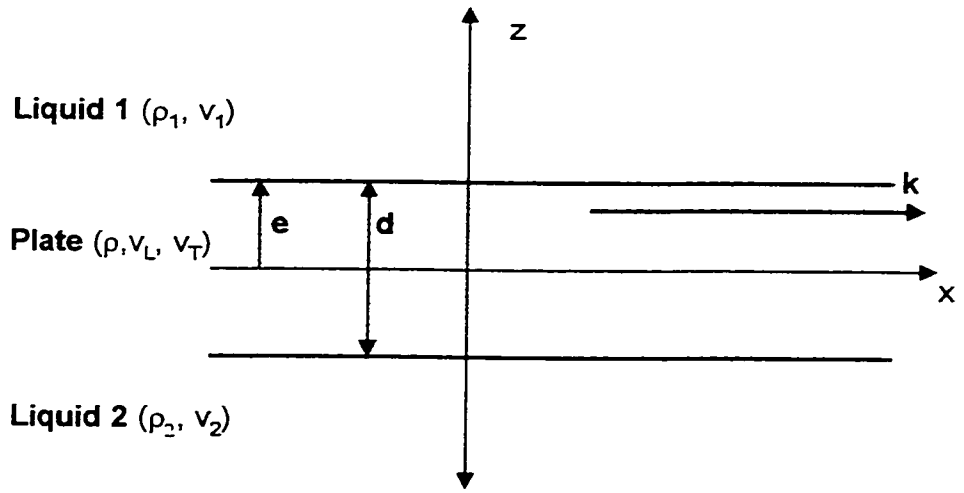

Figure 2.2 Plate configuration

We start with the general equation for a harmonic wave propagating with wave vector $\bar{k}$ in the positive x direction in an arbitrary homogeneous isotropic solid or homogeneous liquid:

$$\left(\nabla^2 - \frac{1}{v_L^2}\frac{\partial^2}{\partial t^2}\right)\varphi = 0 \qquad \text{(Eqn. 2.1)}$$

$$\left(\nabla^2 - \frac{1}{v_T^2}\frac{\partial^2}{\partial t^2}\right)\overline{\Psi} = 0$$

$$\left(\nabla^2 - \frac{1}{v_i^2}\frac{\partial^2}{\partial t^2}\right)\varphi_i = 0 \quad \text{for } i = 1, 2$$

where φ, $\overline{\Psi}$ are the scalar and vector potentials describing particle displacements, $\overline{u}$, in the solid; φ_1 and φ_2 are the scalar potentials in liquids 1 and 2. That is,

$$\overline{u} = \nabla\varphi + \nabla \times \Psi \qquad \text{(Eqn. 2.2)}$$

$$\overline{u}_i = \nabla\varphi_i \qquad \text{for } i = 1, 2$$

We are interested in steady state solutions that are invariant in y so that $\overline{\Psi} = \Psi_z = \Psi$. Eqns. 2.1 become,

$$\frac{\partial^2\varphi}{\partial x^2} + \frac{\partial^2\varphi}{\partial z^2} - k_L^2\varphi = 0$$

$$\frac{\partial^2\Psi}{\partial x^2} + \frac{\partial^2\Psi}{\partial z^2} - k_T^2\Psi = 0 \qquad \text{(Eqn. 2.3)}$$

$$\frac{\partial^2\varphi_i}{\partial x^2} + \frac{\partial^2\varphi_i}{\partial z^2} - k_i^2\varphi_i = 0 \quad \text{for } i = 1, 2$$

where $k_L = \omega/v_L$, $k_T = \omega/v_T$, $k_i = \omega/v_i$ and $\omega = 2\pi f$ (f is the common frequency of the waves in the system). Solutions to Equation 2.3 can be written in the form

$$\varphi(x,z) = \left[A\cosh(R_L z) + B\sinh(R_L z)\right]e^{i(kx-\omega t)}$$

$$\Psi(x,z) = \left[C\cosh(R_T z) + D\sinh(R_T z)\right]e^{i(kx-\omega t)} \qquad \text{(Eqn. 2.4)}$$

$$\varphi_1(x,z) = Ee^{-R_1 z}e^{i(kx-\omega t)}$$

$$\varphi_2(x,z) = Fe^{R_2 z}e^{i(kx-\omega t)}$$

where A, B, C, D, E, F are arbitrary constants, and where [15]

$$R_\gamma = 2\pi f\left(\frac{1}{v_P^2} - \frac{1}{v_\gamma^2}\right)^{1/2}, \text{ for } \mathrm{Re}(R_\gamma) > 0 \text{ for } \gamma = L, T, 1, 2 \qquad \text{(Eqn. 2.5)}$$

For brevity, the factor $e^{i(kx-\omega t)}$ is omitted from the remaining derivation.

Now there is continuity of pressure and particle displacement normal to both plate surfaces, and zero shear stresses in the (non-viscous) liquids parallel to each surface. These boundary conditions are

$$p_{zz} = (p_{zz})_i \text{ for } i = 1, 2 \text{ at } z = \pm e,$$

$$u_z = (u_z)_i \text{ for } i = 1, 2 \text{ at } z = \pm e, \qquad \text{(Eqn. 2.6)}$$

$$(p_{xz})_i = 0 \text{ for } i = 1, 2 \text{ at } z = \pm e.$$

where

$$p_{zz} = \lambda\left(\frac{\partial u_x}{\partial x} + \frac{\partial u_z}{\partial z}\right) + 2\mu\frac{\partial u_z}{\partial z}$$

$$p_{xy} = \mu\left(\frac{\partial u_z}{\partial x} + \frac{\partial u_y}{\partial z}\right).$$

and where λ and μ are Lamé constants. By substituting Equations 2.4 into Equations 2.2 and Equations 2.2 into Equations 2.6, we obtain six equations in the six unknowns A, B, C, D, E and F. These equations can be expressed in matrix form as

$$HA = \begin{bmatrix} a_1 & b_1 & c_1 & d_1 & e_1 & 0 \\ -a_1 & b_1 & c_1 & -d_1 & 0 & f_1 \\ a_2 & b_2 & c_2 & d_2 & e_2 & 0 \\ a_2 & -b_2 & -c_2 & d_2 & 0 & f_2 \\ a_3 & b_3 & c_3 & d_3 & 0 & 0 \\ -a_3 & b_3 & c_3 & -d_3 & 0 & 0 \end{bmatrix} \begin{bmatrix} A \\ B \\ C \\ D \\ E \\ F \end{bmatrix} = 0 \qquad \text{(Eqn. 2.7)}$$

where

$$a_1 = R_L \sinh(R_L e), \qquad c_1 = -ik\cosh(R_T e),$$

$$a_2 = (R_T^2 + k^2)\cosh(R_L e), \qquad c_2 = -2ikR_T \sinh(R_T e),$$

$$a_3 = 2ikR_L \sinh(R_L e), \qquad c_3 = (R_T^2 + k^2)\cosh(R_T e),$$

$$b_1 = R_L \cosh(R_L e), \qquad d_1 = -ik\sinh(R_T e),$$

$$b_2 = (R_T^2 + k^2)\sinh(R_L e), \qquad d_2 = -2ikR_T \cosh(R_T e),$$

$$b_3 = 2ikR_L \cosh(R_L e), \qquad d_3 = (R_T^2 + k^2)\sinh(R_T e),$$

$$e_1 = -R_1 \exp(-R_1 e), \qquad f_1 = R_2 \exp(-R_2 e)$$

$$e_2 = -\frac{\rho_1}{\rho} k_T^2 \exp(-R_1 e), \qquad f_2 = -\frac{\rho_2}{\rho} k_T^2 \exp(-R_2 e).$$

and e = d / 2 is half the thickness of the plate. Solutions for the matrix A exist when the determinant of H equals zero (i.e. |H| = 0). For the case of a plate in vacuum, we have $\rho_1 = \rho_2 = 0$. We can then reduce |H ($\rho_1 = \rho_2 = 0$)| to a product of two determinant $|H_S|$ and $|H_A|$ so that Equation 2.7 becomes

$$|H(\rho_1 = \rho_2 = 0)| = |H_S||H_A| = 0 \qquad \text{(Eqn. 2.8)}$$

where $|H_S| = \begin{vmatrix} a_2 & d_2 \\ a_3 & d_3 \end{vmatrix}$ and $|H_A| = \begin{vmatrix} b_2 & c_2 \\ b_3 & c_3 \end{vmatrix}$.

Equation 2.8 means that there are two independent solution spaces for Equation 2.7 where, respectively, $|H_s| = 0$ and $|H_a| = 0$. These two conditions expand into the characteristic equations for symmetric and antisymmetric motion of a plate first discovered by Lamb:

$$(R_T^2 + k^2)^2 \tanh(R_T d/2) - 4k^2 R_T R_L \tanh(R_L d/2) = 0 \qquad \text{(Eqn. 2.9 a)}$$

$$(R_T^2 + k^2)^2 \coth(R_T d/2) - 4k^2 R_T R_L \coth(R_L d/2) = 0 \qquad \text{(Eqn. 2.9 b)}$$

Equations 2.9 (a) and 2.9 (b) describe two sets of solutions, or two sets of modes of propagation on a plate in vacuum; specifically, the *symmetric* (compressional) and *antisymmetric* (flexural) Lamb modes, respectively. The names "symmetric" and "antisymmetric" refer to the symmetry of particle displacement across the z = 0 plane (see Figure 2.6) [16].

For the case of a plate immersed in a liquid, equations exist that are equivalent to Equations 2.9, except for the addition of a third, perturbation term on the left hand side that arises from the presence the fluid. In the case of a plate in contact with different liquids on each of its surfaces, or for a plate with liquid on one side and air on the other such as in our case, the determinant |H| is no longer separable into a product of two independent determinants. Now, |H| is given by (see derivation in Appendix A):

$$\left|H(\rho_2 = 0)\right| = \left(\left|H_S\right| - \frac{L_{SF}}{2}\right)\left(\left|H_A\right| - \frac{L_{AF}}{2}\right) - \frac{L_{SF}L_{AF}}{4} = 0 \qquad \text{(Eqn. 2.10)}$$

where L_{SF} and L_{AF} are the perturbation terms to the symmetric and antisymmetric equations mentioned above for a plate immersed in a liquid. Were it not for the last term in this equation, the solutions would be separable. In fact, the last term is proportional to the square of the density ratio ρ_1/ρ, and can be ignored for relatively light liquids. In ignoring the final term of Equation 2.10, we have separable solutions for |H| that are equivalent to those for a plate fully immersed in a liquid with density $\rho_1/2$. The resulting approximate characteristic symmetric and antisymmetric equations are Equations 2.11 (a) and (b) respectively:

$$(R_T^2 + k^2)^2 \tanh(R_T d/2) - 4k^2 R_T R_L \tanh(R_L d/2) - \frac{\rho_1 R_L}{2\rho R_L} k^4 \sinh(R_L d/2)\sinh(R_T d/2) = 0$$

$$(R_T^2 + k^2)^2 \coth(R_T d/2) - 4k^2 R_T R_L \coth(R_L d/2) - \frac{\rho_1 R_L}{2\rho R_L} k^4 \cosh(R_L d/2)\cosh(R_T d/2) = 0$$

Equation 2.11 (b) has one real and, in general, many complex solutions for v_p. These solutions must be solved numerically for some pair of values for f and d. Solutions have been found by systematically calculating the generally complex $|H_{AF}| = |H_{AF}|' + i|H_{AF}|''$ over a span of discrete values of v_p' and v_p'', where v_p' and v_p'' are the real and complex parts of v_p (i.e. $v_p = v_p' + iv_p''$). The solution to Equation 2.11 (b) lies at those values of (v_p', v_p'') where $|H_A|' = 0$ and $|H_A|'' = 0$. The above analysis is also true for symmetric modes where we instead solve Equation 2.11 (a) and search for solutions to $|H_{SF}| = |H_{SF}|' + i|H_{SF}|''$.

Figures 2.3 (a) and 2.4 (a) show the dispersion curves ($|v_p|$ vs. fd) for the modes in aluminum and stainless steel plates, respectively. The "A" curves represent Stoneley's real antisymmetric solutions to Equation 2.11 (b) which only exist when the plate is liquid-loaded. The "S_0" and "A_0" curves are the lowest order symmetric and antisymmetric modes in the plate in vacuum, and the "S_0^L" and "A_0^L" modes are the lowest order symmetric and antisymmetric solution in the plate loaded on one surface by water (the "L" stands for "loaded"). Figures 2.3 (b) and 2.4 (b) show the related group velocities, and Figure 2.5 shows the ratio v_p''/v_p' for the A_0^L mode in stainless steel and aluminum plates with water-loading on one side. The values of v_p''/v_p' for the S_0^L mode are essentially equal to zero for values of fd < 1.1 MHz mm. This is equivalent to stating that these modes are not very sensitive to the presence of liquid-loading [5]. Only the supersonic portion (where $v_p > v_1$) of the A_0^L curve is given due to a limitation in the method of solving Equation 2.11 (b) [15].

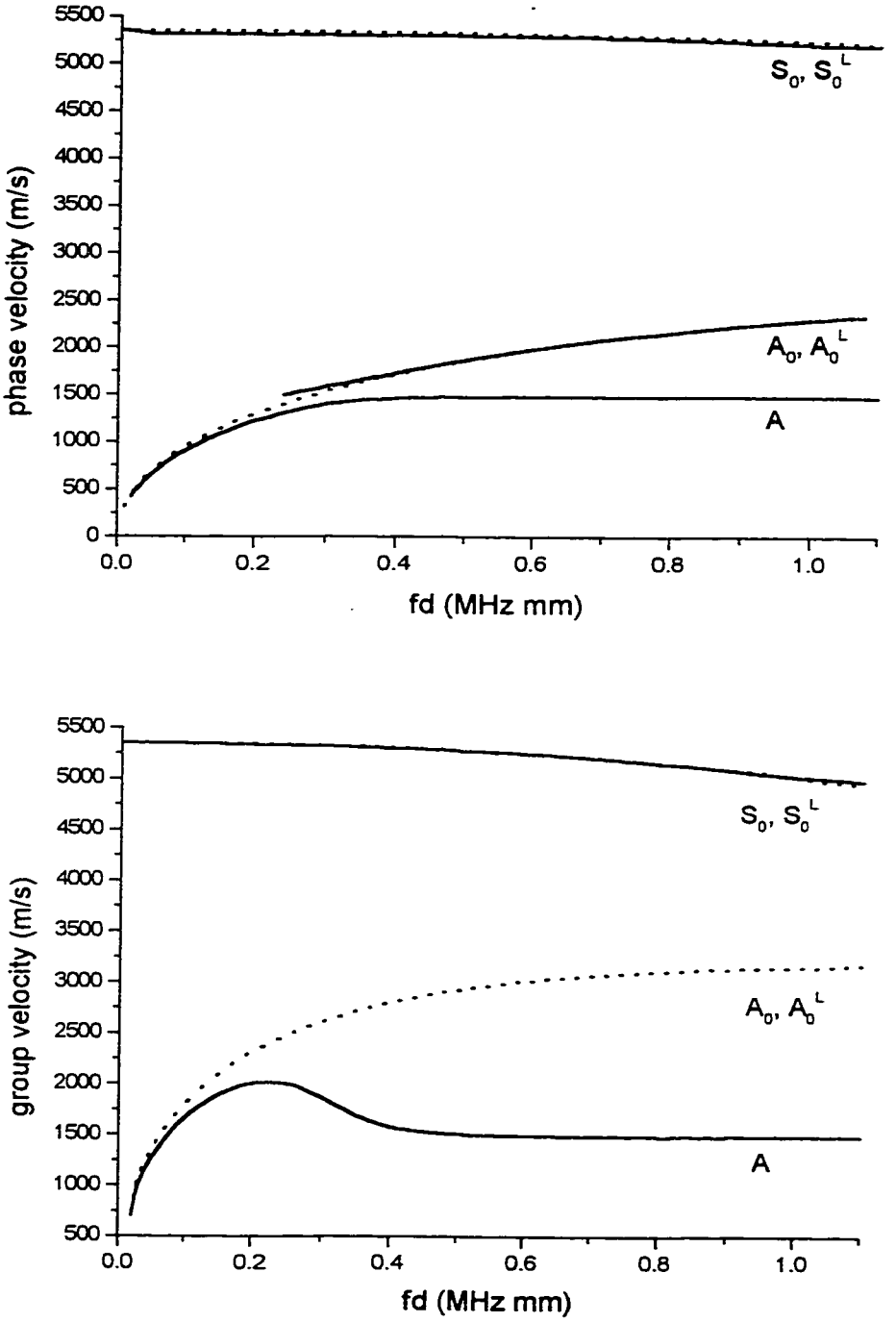

Figure 2.3 Phase and group velocities of lower order Lamb modes in an aluminum plate. The free plate modes A_0 and S_0 are given by dotted lines. The Lamb-like modes A, S_0^L and A_0^L are for the plate loaded by water on one side and vacuum on the other.

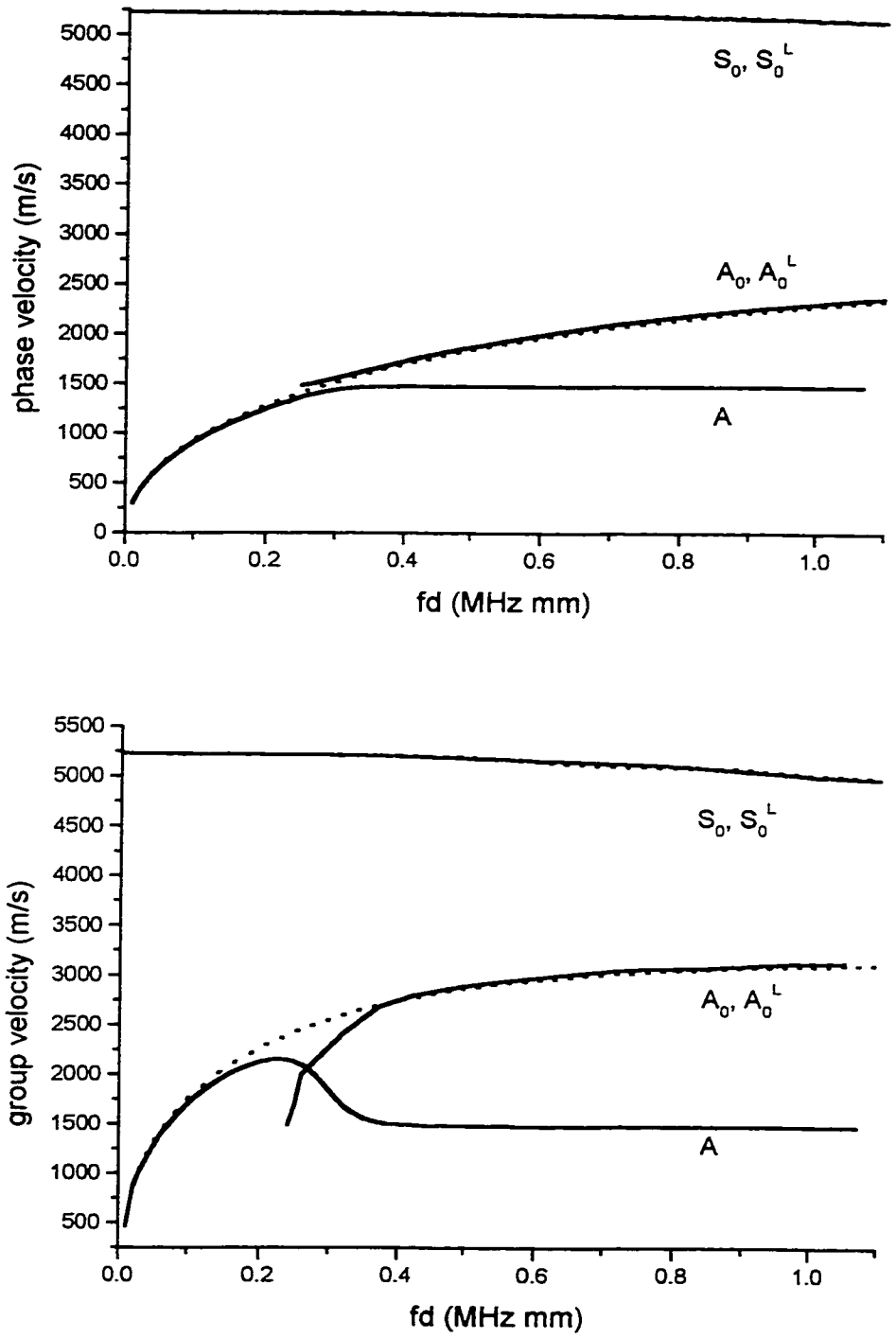

Figure 2.4 Phase and group velocities of lower order Lamb modes in a stainless steel plate. The free plate modes A_0 and S_0 are given by dotted lines. The Lamb-like modes A, S_0^L and A_0^L are for the plate loaded by water on one side and vacuum on the other.

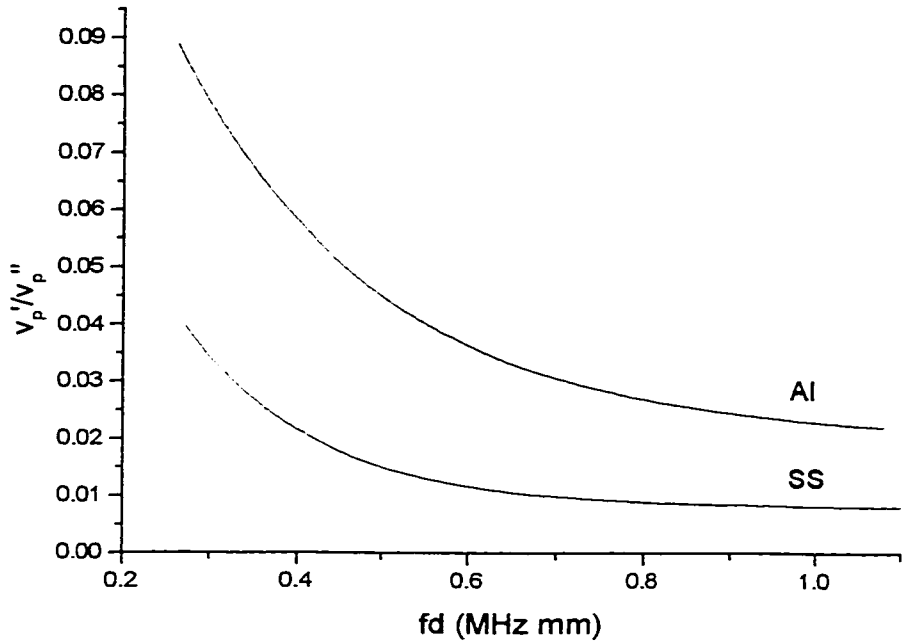

Figure 2.5 Ratio v_p''/v_p' for the A_0^L Lamb-like mode in aluminum and stainless steel plates.

Table 2.1 contains values from these graphs that will be needed when we analyze our experimental data. Notice that the A_0 and A_0^L velocities are treated as equal, as are the S_0 and S_0^L velocities.

	Aluminum	**Stainless steel**		
fd (MHz mm)	0.80	0.64	0.80	0.96
A_0 & A_0^L phase velocity (m/s)	2174	2052	2186	2292
S_0 & S_0^L phase velocity (m/s)	5114	5134	5093	5035
A_0 & A_0^L group velocity (m/s)	3103	3017	3075	3119
S_0 & S_0^L group velocity (m/s)	5114	5134	5093	5035
v_p''/v_p' for A_0^L	0.027	0.011	0.0089	0.0083

Table 2.1 Useful values of the phase velocity, group velocity and imaginary components of Lamb modes in aluminum and stainless steel shells.

2.1.2 Particle displacements

Equations 2.2 and 2.4 give us the components of particle displacements in the plate and in the liquid due to both symmetric and antisymmetric modes. In many situations including our pulsed experiments, however, only one mode such as the A_0^L or S_0^L will exist at any one location at any one time. We are therefore only interested in the particle motions due to the partial, mode-dependent solutions in the plate. The particle motions are plotted in Figure 2.6. Equations for these motions are given in Appendix A. Figure 2.6 clearly shows the symmetric and antisymmetric nature of these modes – notice that the symmetric mode is a mirror image about the z = 0 plane, and the antisymmetric mode have diametrically opposite motions across the z = 0 plane. Also notice the compressional waves that radiate off into the liquid at specific angles (θ_{S0} and θ_{A0}, respectively) to the plates.

(a)

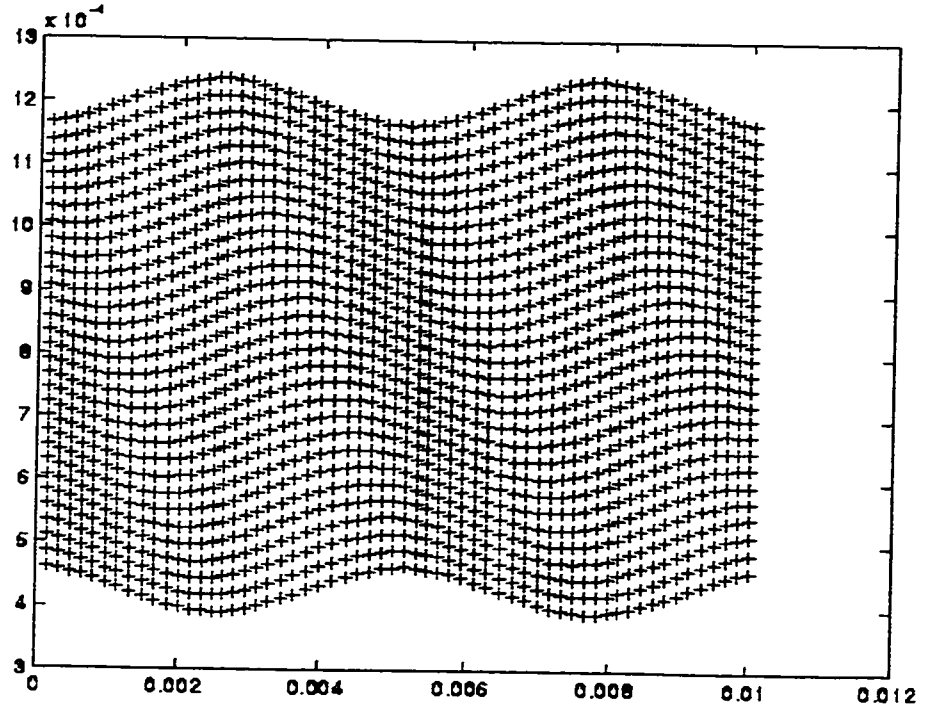

(b)

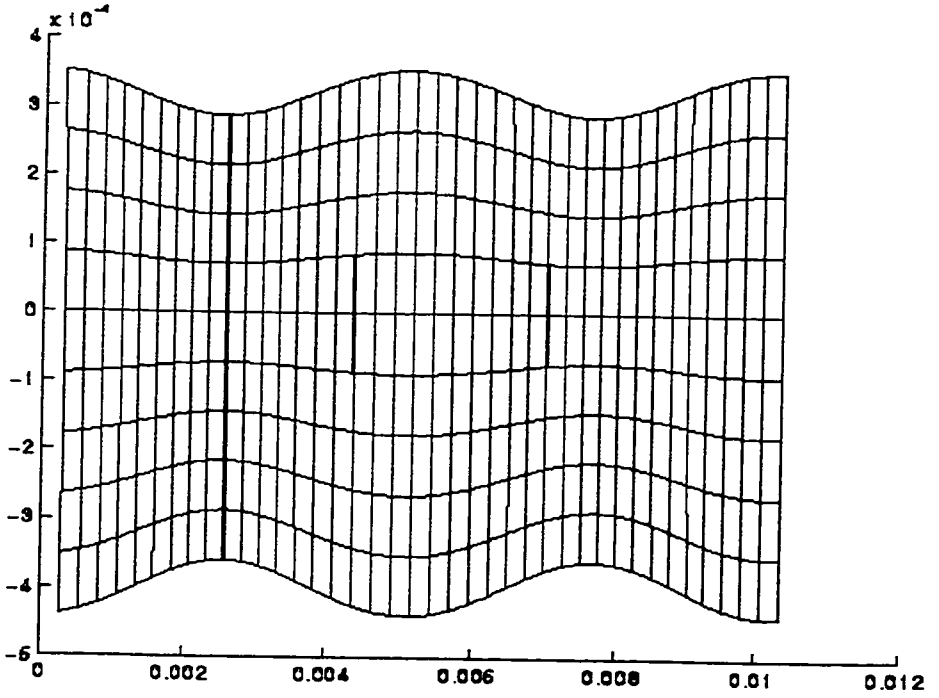

Figure 2.6 (a) & (b) Particle displacement for the lowest order symmetric mode in an 0.8 mm aluminum plate at 1.0 MHz, (a) liquid motion above plate, (b) plate motion.

(c)

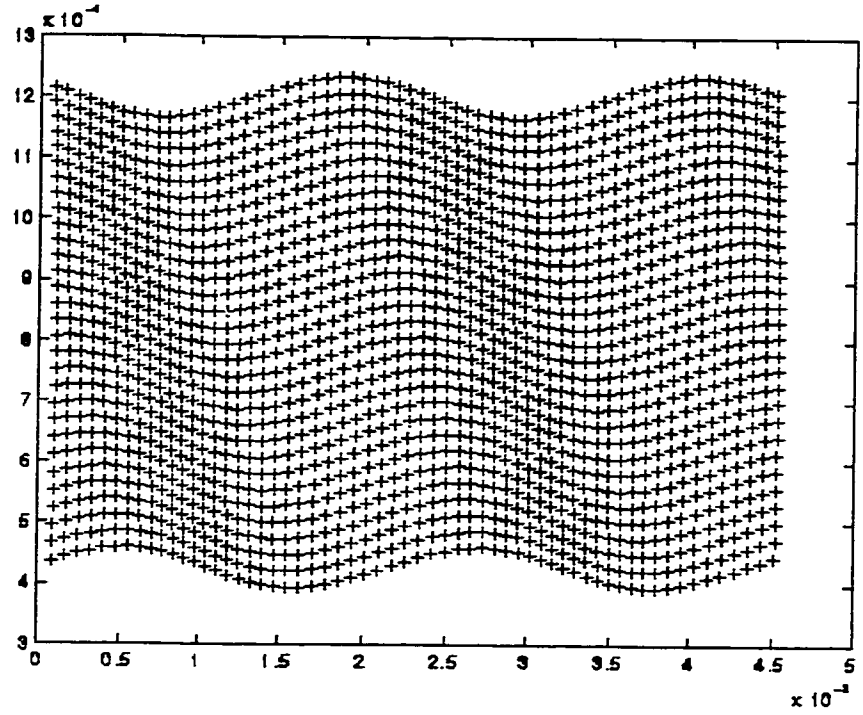

(d)

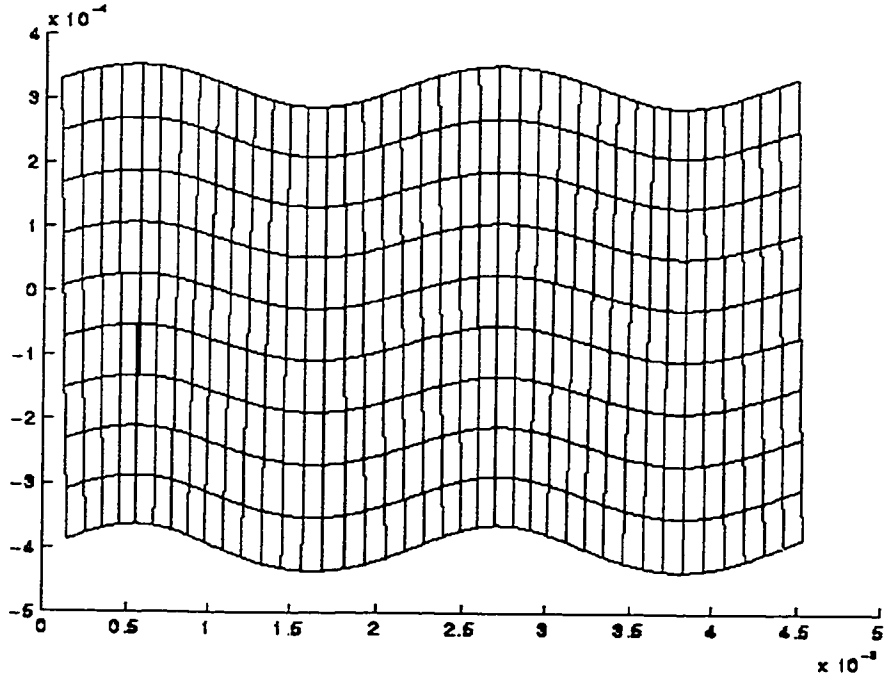

Figure 2.6 (c) & (d) Particle displacement for the lowest order antisymmetric mode in an 0.8 mm aluminum plate at 1.0 MHz, (c) liquid motion above plate, (d) plate motion.

2.1.3 Attenuation and energy leakage

The attenuation of a wave over some distance, x, is simply the ratio of its final pressure, A_f, to its initial pressure, A_i. Attenuation is an exponential phenomenon, so that

$$A_f = A_i e^{-\alpha x}$$

where α is the *attenuation coefficient* [Nepers/m] . α is given by the imaginary component k″ of the wave number k = k′ + ik″ [15]. k″ is a function of v_p''/v_p' such that

$$k'' = 2\pi f \frac{v_p''}{v_p^{\,2}} \qquad \text{(Eqn. 2.12)}$$

Attenuation of Lamb-like waves in a liquid-loaded plate arises mainly due to radiation of acoustic energy into the liquid [17, 18]. Lamb-like modes are, therefore, often referred to as a "leaky" modes.

Energy leaked from the A_0^L and S_0^L Lamb waves do so at a specific angles, θ_{A0} and θ_{S0}, respectively, to the plate normal according to Snell's law [19],

$$\sin\theta_i = \frac{v_1 \sin\theta_i}{v_i} = \frac{v_1}{v_i},\ i = A_0^L,\ S_0^L \qquad \text{(Eqn. 2.13)}$$

where v_1 is the speed of sound in the liquid. Notice that in the subsonic regime where $v_{A0L} < v_1$, θ_{A0} is not purely real. The A_0^L mode therefore can not leak into the ambient liquid in this regime, nor can an incident wave generate the A_0^L mode in the plate [20].

Table 2.2 lists some results that will be needed for our analysis of the experimental data. The attenuation distance listed in Table 2.2 provides us with a measure of the effective beam width of the leaked energy. Some measure of beam width is needed for comparison with the dimensions of the system so that it can be determined whether the approximation of ray acoustics is valid. Ray acoustics can be used in our case only where the beam width is small with respect to the geometry of the system. This will be discussed in greater detail in Chapter 4.

	Aluminum	**Stainless Steel**		
fd (MHz mm)	0.8	0.64	0.8	0.96
A_0^L attenuation coef. (Neper/m)	78.0	26.9	25.6	27.3
A_0^L attenuation distance (- 20 dB) (mm)	29.5	85.5	89.8	84.2
A_0^L leaky angle	43.0^0	46.3^0	44.1^0	40.3^0

Table 2.2 Parameters related to the attenuation of Lamb modes in aluminum and stainless steel plates.

2.1.4 Reflection and reemission of bulk waves

The ratio of reflected pressure to incident pressure for a wave incident upon an liquid-solid interface is given by the *reflection coefficient*, V. Brekhovskikh [21] defines V for a boundless plane wave incident in liquid upon a plate with vacuum (air) on the other side (Equation 2.14). Figure 2.7 shows the reflection coefficient versus angle of incidence for a water/aluminum/vacuum system.

$$V = e^{i\phi} \text{ where} \qquad \text{(Eqn. 2.14)}$$

$$\phi = 2\arctan[(MZ_1)Z_3]/[(MZ_1)^2 - (NZ_1)^2],$$

$$MZ_1 = Z_2 \cos^2 2\gamma_2 \cot(k_2 d\cos\theta_2) + (Z_{2t}/Z_t)\sin^2 2\gamma_2 \cot(\kappa_2 d\cos\gamma_2)$$

$$NZ_1 = Z_2 \cos^2 2\gamma_2 / \sin(k_2 d\cos\theta_2) + Z_{2t} \sin^2 2\gamma_2 / \sin(\kappa_2 d\cos\gamma_2)$$

$$Z_2 = \rho_2 v_L / \cos\theta_2,\ Z_{2t} = \rho_2 v_T / \cos\gamma_2 \text{ and } Z_3 = \rho_3 v_3 / \cos\theta_3$$

and where θ_3 is the angle of incidence; k_2 and θ_2 (resp. κ_2 and γ_2) are the wavenumbers and refraction angles of the longitudinal (resp. transverse) wave in the solid; and d is the thickness of the plate.

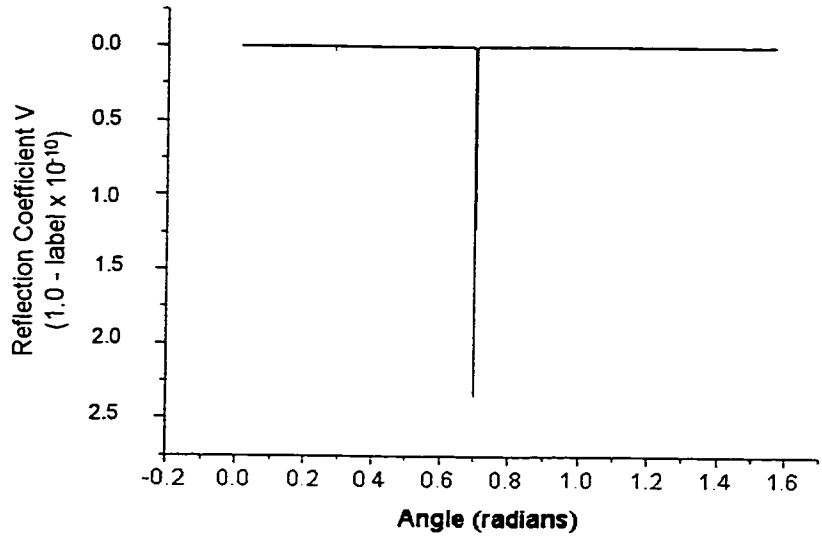

Figure 2.7 Reflection coefficient vs. angle of incidence for a plane wave incident in water upon an aluminum plate at fd = 0.8 MHz mm.

While V is essentially equal to 1 at all angles, there is an interesting small dip at the angle where, by Snell's law (Equation 2.13), the refracted wave would travel down the plate with velocity $v_P = v_{A0L}$ = 2174 m/s. This is no accident, say Chimenti *et al*, who make the connection between the minimum in the reflection coefficient and the lowest

order flexural Lamb-like mode in an aluminum plate immersed in water [22]. Mott identified a similar minimum at the Rayleigh angle for a plane wave incident in water onto the surface of a semiinfinite solid (steel) [23].

The reflection coefficient generally provides a good indication of the amount of energy that is scattered from a surface. This is not the case, however, for a plate where Lamb-like waves are generated by the incident wave. This is because Lamb-like waves leak into the liquid π out of phase with and at the same angle as the reflected wave, causing destructive interference [17, 23]. In 1952, Schoch observed this reflected / reemitted beam, which he misinterpreted as a "lateral displacment" of the reflected beam originating from a solid half-space [24]. Deighton *et al* derived an equation for the conversion efficiency for a plane wave incident in liquid at the critical angle onto a plate over a distance 'a' [17]:

$$\text{The efficiency } \eta = \frac{P_{SAW}}{P_i} = \frac{2(1-e^{-\alpha a})^2}{\alpha a} \qquad \text{(Eqn. 2.15)}$$

where P_i is the total power of incident wave and P_{SAW} is the total power of the Lamb-like wave that is generated. The remaining power is reflected / reemitted so that [17]

$$\frac{P_{R/R}}{P_i} = 1 - \eta = 1 - \frac{2(1-e^{-\alpha a})^2}{\alpha a} \qquad \text{(Eqn. 2.16)}$$

is the proportion of the energy returned to the liquid over the distance 'a'. The effective pressure transmission coefficient and pressure reflection / reemission coefficient are proportional to the square root of η and 1- η, respecitvely.

We can apply Deighton's results to our curved system when we make the conceptual transformation shown in Figure 2.8. In our system, the cylinder wall acts as both emitter and receiver of bulk waves in the liquid. Figure 2.8 (a) shows that waves are always emitted and received at the critical angle (θ_{A0} if emitted from the A_0^L mode), and that this condition is respected by the "flattened" system shown in Figure 2.8 (b). Both plates 1 and 2 are similar to Deighton's flat plate.

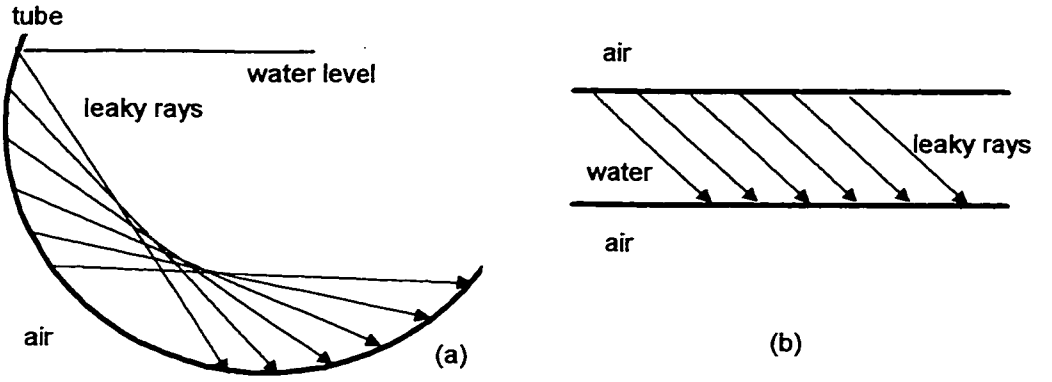

Figure 2.8 "Flattening" of shell wall (a) to two parallel plates (b)

2.1.5 Action at a loading interface

Here we are interested in knowing the amount of reflection and transmission of a Lamb wave as it makes the transition past an air-liquid boundary.

Feit *et al* [25] calculated the two dimensional near-field response of a steel plate loaded by water on one of its surfaces and by air on the other and driven by a uniform line source set perpendicular to the saggital plane. These calculations were performed in

both the subsonic and supersonic regimes. In the subsonic regime, the source was found to cause two distinct waves: an evanescent wave that travels without attenuation in the water along the plate surface, and a cylindrically spreading bulk wave in the water emanating from the line source. Similarly, the supersonic regime saw to the generation of a (non leaky) interface wave and the cylindrically spreading wave. It was shown that the supersonic leaky wave diminished significantly in amplitude as it traveled down the plate. The leakage of this interface wave interferes destructively with the cylindrically spreading wave, causing pressure lobes along a line that extends out from the plate at 45^0 to its surface.

Matula *et al* [26] experimentally confirmed Feit's findings for the subsonic regime using an aluminum plate that was partially immersed in water. A pulse of subsonic (relative to the sound velocity in water) A_0 Lamb wave was generated in the free portion of the plate. This wave traveled down the plate into the water, where near field scattering was observed. An important result is that no significant reflection of the pulse from the water's surface was observed.

2.2 Circumferential modes

We now consider modes that only exist in shells containing a liquid core. These modes are characterized by the coupling of the modes in the two subsystems shown in Figure 2.9: (a) the A_0 Lamb mode in an empty cylindrical shell and (b) whispering gallery modes in the internal water column. Whispering gallery modes were first reported by Lord Rayleigh [27]. Veksler *et al* note the rather important result that the whispering gallery modes propagate without attenuation [5]. This implies that they do not leak into the liquid core.

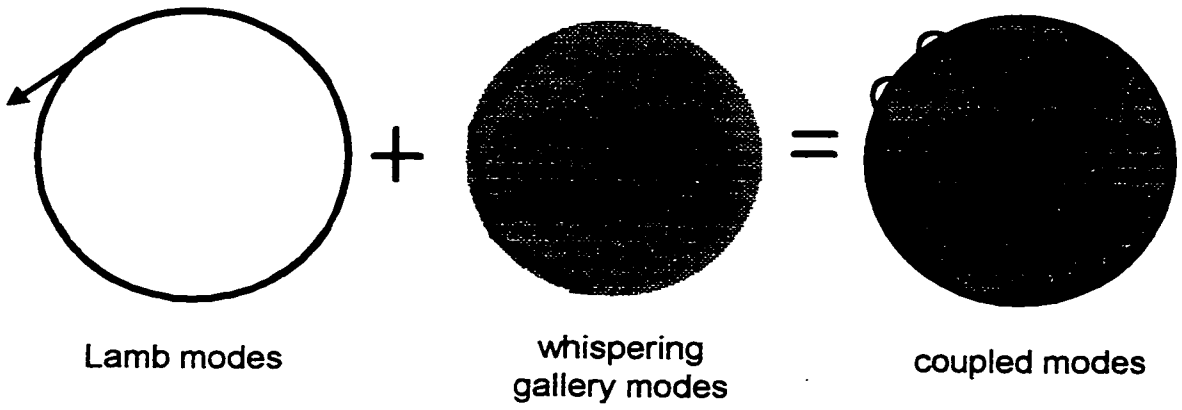

Figure 2.9 Curved subsystems and the modes they support.

It would happen that at certain values of fd, the velocities of some Lamb modes in the shell would equal the velocities of whispering gallery modes in the adjacent water column. In the coupled system, the modes in the two subsystems exhibit *mode repulsion*. Figure 2.10 illustrates mode repulsion in a water-filled stainless steel shell [28]. We see there that the dispersion curves for the modes of the coupled system, C1 and C2, do not cross, rather veer away from one another to follow the velocity curves of the subsystems when these are sufficiently different from one another.

While the phase velocities of the coupled modes do not differ much from v_{A0} in the coincidence regions, their group velocities do. Figure 2.11 show the group velocities for the modes shown in Figure 2.10. The curves in Figure 2.11 were confirmed by Cheeke *et al* who observed the coupled mode group velocities where they plateau, i.e. where 0.21 MHz mm < fd < 0.6 MHz mm [29]. Clear echoes could not be obtained outside this fd region. Talmant was also unable to observe clear echoes for Lamb-like modes in submerged plates [30].

We can see that the group velocities of Figure 2.11 differ considerably from those of the Lamb-like modes of Figure 2.3. Because of this difference, a pulse's total flight time back to the transducer will be significantly different depending on whether it propagates in the loaded portion of the shell as a coupled mode or as a Lamb-like mode. We must consider both flight times when, in Chapter 4, we compare the theoretical flight times with experimental times.

Figure 2.11 does not provide us with the group velocities at our experimental values of fd = 0.64, 0.8 and 0.96. If indeed coherent pulses do exist at these upper regions of fd, we assume that the group velocities would be similar to the plateau velocities of 2400 m/s shown in Figure 2.11. Values for the velocities in a water-filled aluminum shell could not be found in the literature.

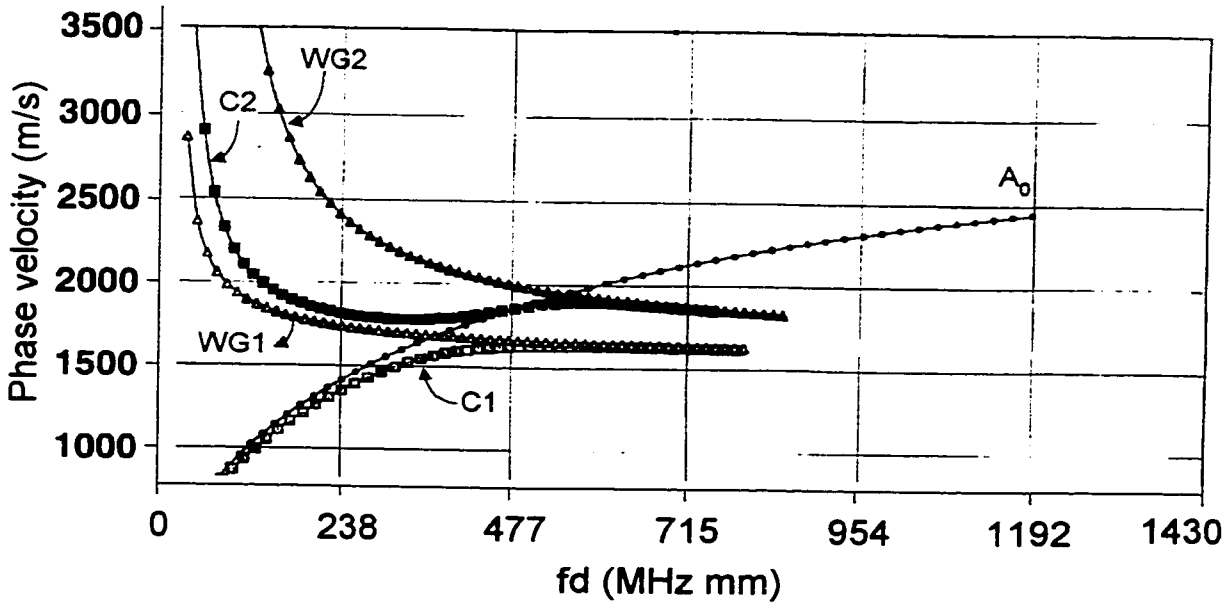

Figure 2.10 Theoretical phase velocities of modes in a water-filled stainless steel shell and its subsystems: A_0 is a Lamb mode in empty shell; C1 and C2 are first two coupled modes of water-filled shell; WG1 and WG2 are first two modes in water column. Shell outer radius = 9.8 mm, wall thickness = 0.254 mm [28].

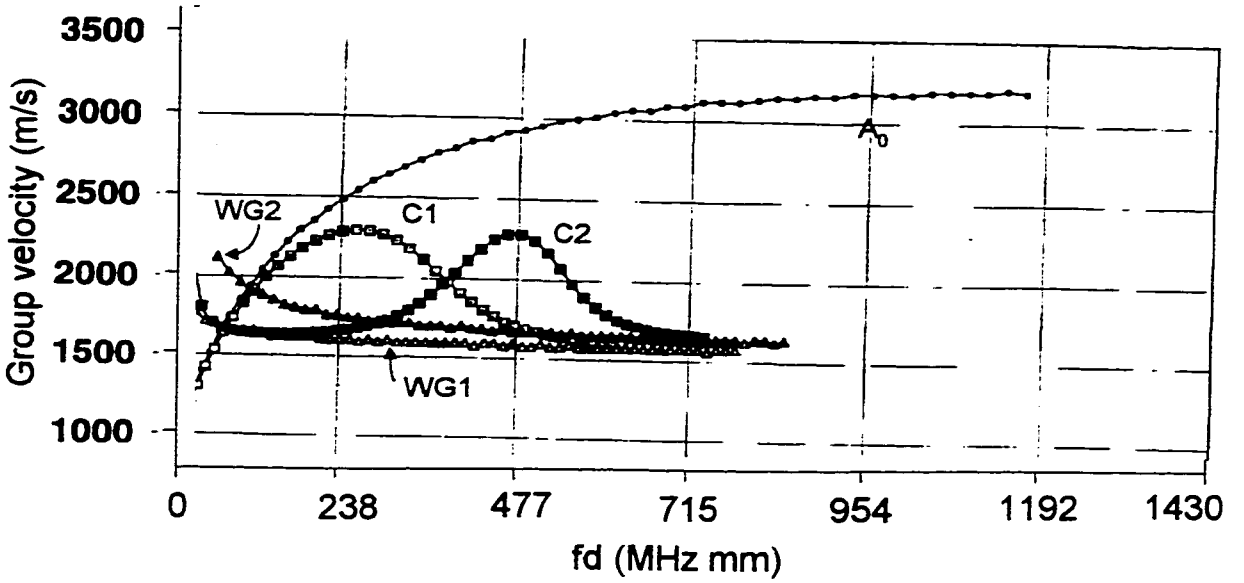

Figure 2.11 Theoretical group velocities of modes in a water-filled stainless steel shell and its subsystems. A_0 is lowest order Lamb mode in empty shell; C1 and C2 are first two coupled modes of water-filled shell; WG1 and WG2 are first two modes in water column. Shell outer radius = 9.8 mm, wall thickness = 0.254 mm [28].

3. EXPERIMENT

We performed three types of experiments in this research. The main experiment of course was (a) the *pulse-echo experiment* where multiple echoes were received when a single pulse was input to the system. The other two experiments were designed to determine which modes propagate in the shells:

(b) *Phase velocity experiment*: A pseudo-continuous acoustic wave was input to the system instead of an acoustic pulse. This experiment used interference effects to measure the phase velocity of the A_0 mode in the empty shells.

(c) *Obstruction experiments*: Objects were placed in the system so as to obstruct specific acoustic pathways. These experiments consisted of hanging objects inside the liquid filler, and placing objects in contact with the outer surface of the cylinder below the water line in order to dampen any modes that may be propagating in the cylinder wall.

3.1 Shells and frequencies

One aluminum and one stainless steel shell were tested, with the aluminum shell being tested at one frequency and the stainless steel shell tested at three frequencies. Shell sizes and frequencies are listed in Table 3.1.

	Aluminum	Stainless Steel
Inner radius (mm)	45.1	14.85
Outer radius (mm)	45.9	15.25
Shell Circumference (mm)	285	94.6
Wall thickness, d (mm)	0.8	0.8
Frequency, f (MHz)	1.0	0.8, 1.0, 1.2
fd (MHz mm)	0.8	0.64, 0.8, 0.96

Table 3.1 Shell parameters

For the experiment to yield meaningful results, the pulse parameters must be suited to the size of the system. For instance, to distinguish between leaky and non-leaky modes, the attenuation distance of the leaky modes must be considerably smaller than the total submerged portion of the shell. That is, the leaky mode must have enough water-loaded shell in which to leak. Table 3.2 compares key shell and pulse distances.

	Aluminum	Stainless Steel		
fd (MHz mm)	0.8	0.64	0.8	0.96
Cycles / burst	13	13	13	13
Pulse duration (μs)	13	16.3	13	10.8
A_0 & A_0^L wavelength (mm)	2.2	2.6	2.2	1.9
S_0 and S_0^L wavelength (mm)	5.1	6.4	5.1	4.3
Lowest coupled mode wavelength (mm)	1.8	2.3	1.8	1.5
- 20 dB A_0^L leaky distance (mm)	29.5	85.5	89.8	84.2

Table 3.1 Pulse parameters

All experimental points are in the supersonic regime for the A_0, A_0^L, S_0, S_0^L and whispering gallery modes.

3.2 Experimental configuration

Except perhaps for transducer placement and coupling, this research uses an experimental configuration (shown in Figure 3.1) that is basic to applications in nondestructive testing (NDT) of materials and structures by contact ultrasonic and pulse-echo techniques [31]. A Ritec RAM-10000 pulser-receiver system was used to generate and receive the pulses. The Ritec amplified the received signals, and fed them to a digital oscilloscope for display and time averaging. The oscilloscope was connected via GPIB bus to a computer for signal acquisition and recording.

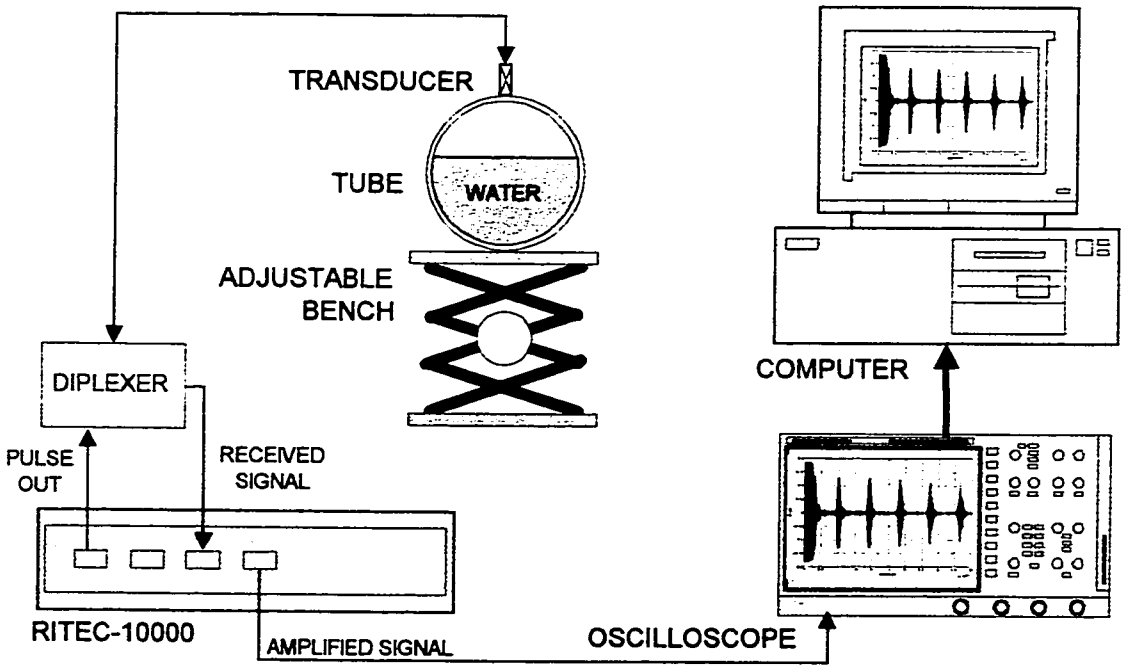

Figure 3.1 Experimental setup

In each experiment, the transducer was placed atop the shell's outer wall. Two different transducers were used: a 0.5″ diameter 1.0 MHz narrowband immersion transducer (Panametrics® Model A303-5) was used on the aluminum shell. A 1.0″ diameter 1.0 MHz wideband (0.6 MHz bandwidth) was used on the stainless steel shell (Matec® Model 1L0108HR). In each case, the transducer was coupled to the cylinder by a thin line of Sonotrace 30® ultrasonic couplant carefully deposited parallel the cylinder's main axes. Waves were emitted from this coupling mainly in the circumferential directions.

3.3 Pulse-echo experiment

The pulse-echo experiments were performed in the following steps.

1. The Ritec was configured to the appropriate frequency, and voltage.

2. The transducer was coupled to the empty tube so as to produce the A_0 mode. The transducer never touched the shell. The height of couplant (the distance between the transducer and cylinder) could be adjusted by means of the adjustable bench shown in Figure 3.1. It was found that different echo patterns were obtained by changing the coupling height while the Ritec was in operation, and that the A_0 mode, in particular, could be preferentially generated and received in the empty tube at a particular coupling height. That the A_0 mode was indeed being generated was verified by (i) measuring the time delay, Δt, between echoes using cursors on the oscilloscope, (ii) calculating the group velocity for circumferential propagation $v_g = 2\pi r/\Delta t$, where r is the average radius of the shell, and (iii) comparing this experimental velocity with the theoretical velocities for the A_0 and S_0 modes.

3. Waveforms were acquired in the empty and partially water-filled cylinder. Water was first added to the cylinder to a height of 4/18 of the cylinder inner diameter. Below this level, most echoes were hidden in noise. Great care was taken not to modify the couplant when adding the water so that the A_0 mode would continue to be generated when the shell contained water. The water was then added in steps of $1/18^{th}$ or $1/36^{th}$ of the cylinder diameter (in the stainless steel and aluminum cases, respectively) to a maximum height of 17/18 in the stainless steel shell and 35/36 in the aluminum shell. A waveform was acquired at each fill height.

4. The signals were filtered. The poor impedance match of the immersion transducers to the thin line couplant is marked by the presence of considerable harmonics in the received signal as shown in Figure 3.3 (a). The signals were therefore filtered using Labview's® bandpass filters with 0.2 MHz bandwidth.

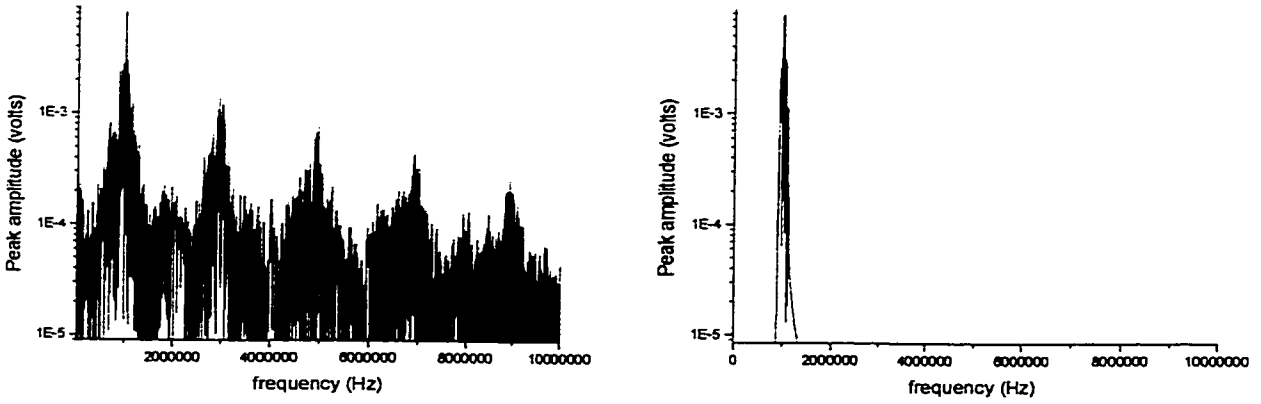

Figure 3.2 Typical waveform spectrum: (a) unprocessed and (b) after 0.2 MHz bandpass filter.

5. Peaks in the signal were identified. A program was written in Matlab® to find the points of maximum amplitude in the filtered signals using an 8 μs [800 sample pts.] moving window, with the results being written to a database. The program could identify maxima separated by at least 8 μs.

3.4 Phase velocity experiment

We were able to measure the phase velocity of the mode generated in the empty cylinder by:

1. Producing pulses of the A_0 mode at as described above in step 2 of Section 1.3.

2. Increasing the cycles per burst (CPB) until there was significant overlap in the pulses, and acquire a waveform.

3. We repeated step 2 at 10 frequencies spaced in small increments $\Delta f = 0.005$ MHz about the center frequency.

4. We plotted the average power of the signals taken at each frequency.

The average power passes through a series of local maxima and minima over the tested frequency range. The minima correspond to frequencies at which signals propagating around the shell interfere most destructively with the signal being generated by the transducer, i.e. differ in phase by nλ/2 so that $n\lambda / 2 = 2\pi r$ where λ is the wavelength of the A_0 mode, n = is an odd integer, r is the shell radius and $2\pi r$ is the path difference of wavecrests under the transducer. It follows that adjacent minima correspond to adjacent n's, i.e. $n_{i+1} = n_i + 2$, and that adjacent frequencies differ by

$$\Delta f_{min} = f_{i+1} - f_i = \frac{v_p}{\lambda_{i+1}} - \frac{v_p}{\lambda_i} = v_p\left(\frac{n+1}{2\pi r} - \frac{n}{2\pi r}\right) = \frac{v_p}{2\pi r} \qquad \text{(Eqn. 3.1)}$$

Therefore,

$$v_p = 2\pi r \Delta f_{min} \qquad \text{(Eqn. 3.2)}$$

3.5 Obstruction experiments

The aim of the obstruction experiments was to specifically test which paths were taken by the acoustic energy through the system. This was done by obstructing the paths through the water or along the shell wall, and comparing the waveforms acquired from shells with and without the obstructions. The obstructions tested for the presence of:

- *Through transmission*: "Through transmission" refers to the transmission of acoustic energy straight through the interior of the shell. This energy reflects off the bottom shell wall back to the transducer. The aim of this test was to determine whether there was direct transmission from transducer to the liquid when a shell is fully filled with water. With the Ritec active, a flat plate was placed in the full shell and moved to various positions and orientations, while the oscilloscope was monitored for any changes in waveform.

- *Leaky modes*: Leaky modes would be marked by the radiation of acoustic energy off the internal shell wall. Among the modes considered in this research, only the A_0^L would theoretically be leaky in our experimental fd region. Leaky modes would then be marked by the presence of bulk waves in the liquid interior, and could be

identified indirectly by observing these bulk waves. Objects such as paper clips and razor blades were therefore hung inside the shell so that they came near but did not touch the shell wall. With these obstructions in place, the pulse-echo experiment was performed at a number of fill levels. The waveforms so produced were compared to those from the non-obstructed shell. Differences from the non-obstructed waveform would mean that the acoustic path does include a trip through the liquid, and that leaky modes exist in the shell.

- *Circumferential modes*: "Circumferential modes" refer to those modes that travel exclusively around the shell wall. These modes would include the S_0^L and coupled modes. To detect circumferential modes, the external wall of the stainless steel shell was touched with different objects at various points far below the water line. Objects included a rubber band, a wet cotton swab, a finger, water droplets and (ahem) a large lump of peanut butter.

4. RESULTS AND ANALYSIS

This chapter presents the results of the experiments described in Chapter 3 and develops the steps taken to identify the paths of the acoustic pulses through the system. The aluminum and stainless steel shells will be analyzed in turn. For each shell, we first inspect the waveforms from the empty shell to ensure that we are generating the A_0 mode. We then analyze the data for the partially-filled shell by (a) identifying the time spacing for periodically occurring echoes, (b) comparing these experimental periods to theoretical flight times for various paths in order to match periods with flight paths. We thus aim to identify the path taken through the system. Any conclusions are checked with the results of the obstruction experiment.

4.1 Aluminum shell

In this section we describe results of the pulse-echo experiment and supporting experiments on the aluminum shell at 1.0 MHz. The experiments themselves, including any signal processing, were described in Chapter 3.

Figure 4.1 is a waterfall plot of the experimental data gathered from the aluminum shell. The plot shows all thirty six (rectified) waveforms acquired from the aluminum shell. Each waveform corresponds to a different fill level, with '0' referring to the empty shell, and '35' referring to the (almost) full shell (note that a waveform was not acquired for the full tube due to strong through transmission). Figure 4.1 seems to exhibit at least one family of echoes whose period increases with the liquid height. Unfortunately, things aren't that simple. Inspection of the individual waveforms will show that these

echoes do not increase monotonically in period with liquid height, and actually take a number of different paths around the system.

We proceed next to examine the waveforms for the empty shell and some exemplary waveforms taken when the shell was partially-filled with water.

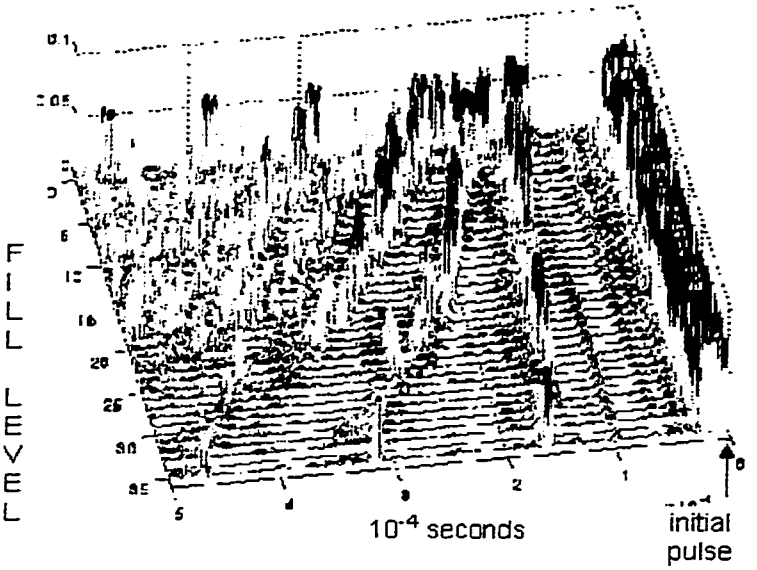

Figure 4.1 Waterfall plot for the 36 waveforms acquired on the partially water-filled aluminum shell

4.1.1 Empty shell group velocity

Figure 4.2 shows the waveform acquired when the shell was empty. Here we can see a clear echo train with a constant period of 92.3 μs between adjacent echoes, corresponding to a group velocity of 3096.9 m/s around the circumference of the shell.

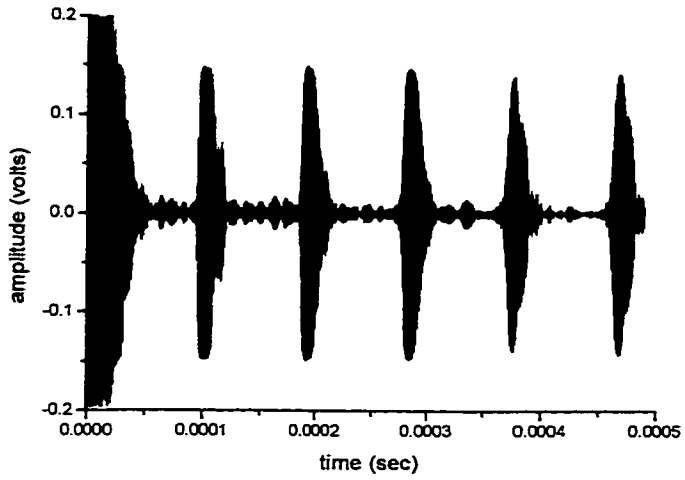

Figure 4.2 Filtered waveform for the empty aluminum shell

4.1.2 Empty shell phase velocity

We obtained rather curious results from this experiment. The experiment was performed a number of times, and every time produced a frequency spacing, Δf_{min} in Equation 3.1, equal to 0.02 MHz. This provides us with an experimental value for the phase velocity v_p in Equation 3.2 equal to 3192 m/s. This experimental value actually equals the theoretical group velocity. It seems that we have unwillingly measured the group velocity. Details of the experiment and analysis of results for both the aluminum and stainless steel shells can be found in Appendix B.

4.1.3 Partially-filled shell

Distinct echoes can be seen in all the waveforms acquired when the water was above the height of 4/36D, where D is the shell's inner diameter. These echoes often exhibit patterns in which three or more echoes are separated from one another by the same

amount of time. We assume that such a pattern is not accidental, and that it most likely results from a pulse repeatedly circumnavigating the system, producing an echo each time it passes under the transducer.

Our aim is to identify the origin of the patterns in terms of specific paths taken through the system. Using a computer simulation to aid with the tedious task of tracking a hypothetical pulse through the system, the path for approximately 70% of all the echoes observed in the aluminum shell have been identified. Illustration of the paths for every pattern would be unnecessarily heavy. Instead, we limit our explanation to the patterns at three fill levels. The waveforms acquired at fill levels ¼D, ½D and 25/36D are shown in Figures 4.3, 4.4 and 4.5. Table 4.1 lists the periods of the patterns identified in the figures.

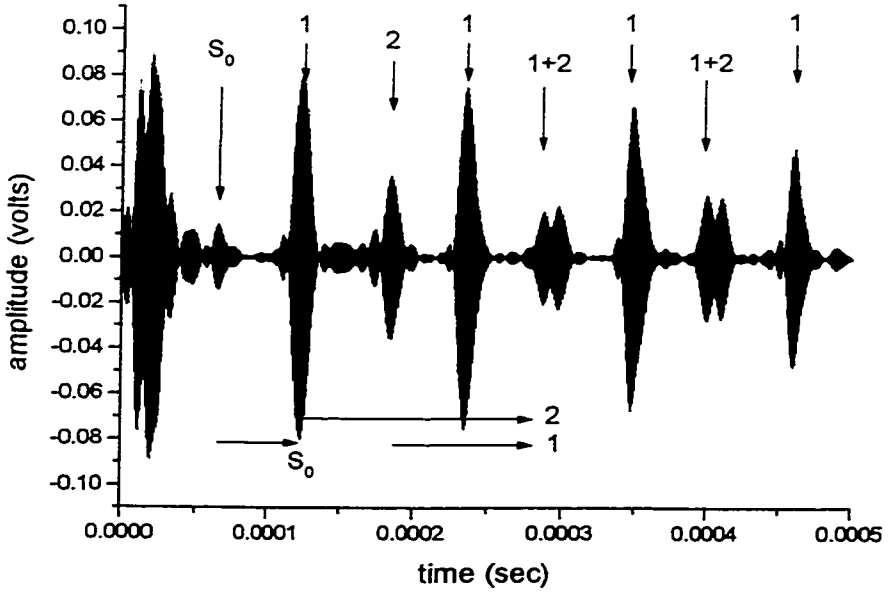

Figure 4.3 Waveform acquired at 1.0 Mhz from the aluminum shell ¼ full of water. Four repetitive patterns are identified and labeled S_0, 1, 2, and 1+2. These arise from three periods (horizontal arrows) S_0, 1 and 2.

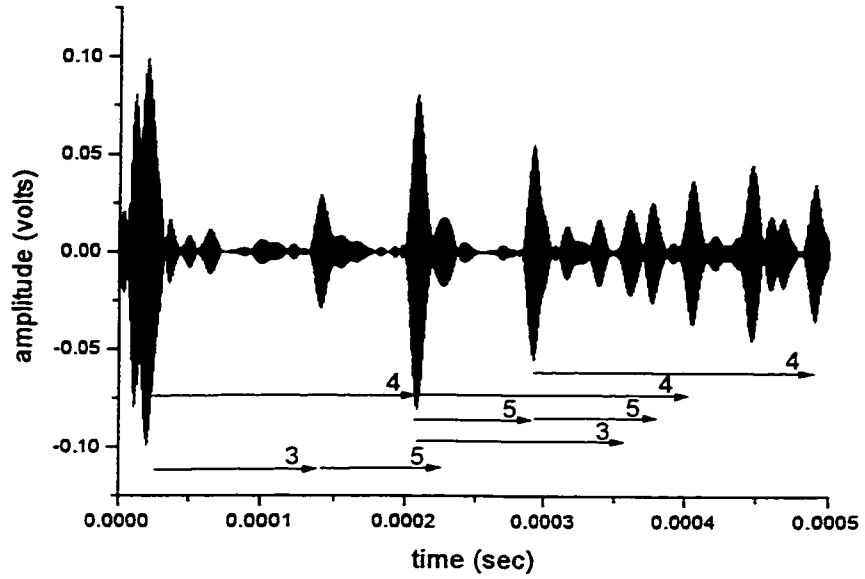

Figure 4.4 Waveform acquired at 1.0 MHz when aluminum shell was ½ full of water. Periods 3, 4 and 5 are identified.

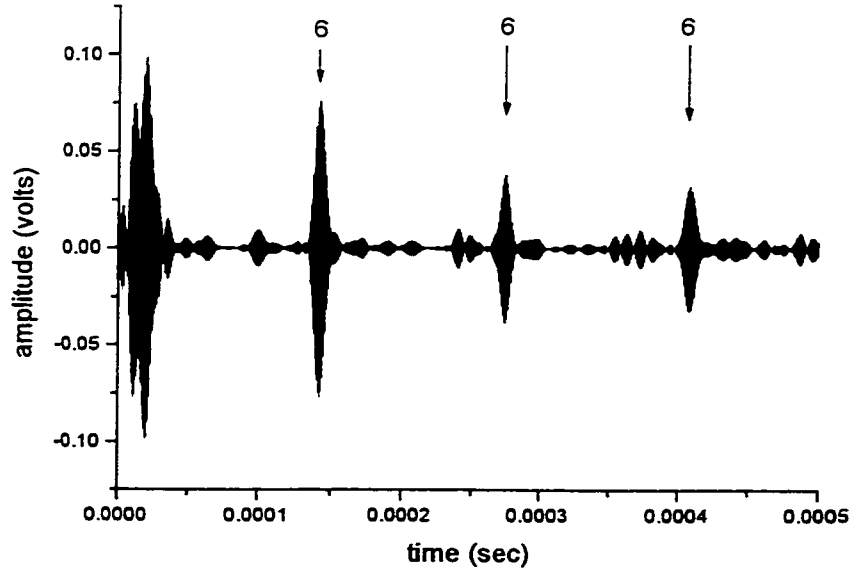

Figure 4.5 Waveform acquired at 1.0 MHz when aluminum shell was filled with water to a height of 25/36 of the shell diameter (approximately 2/3rd full)

¼ Fill		½ Fill		25/36 Fill	
Pattern	Period (μs)	Pattern	Period (μs)	Pattern	Period (μs)
1	111.77 ± 1.1	3	130.5 ± 1.3	6	133.4 ± 0.5
2	163.3 ± 0.3	4	197.5 ± 1.5		
S_0	56.1*	5	84.1 ± 0.8		

Table 4.1 Periods of the echoes acquired from the aluminum shell at 1.0 MHz when ¼, ½ and 25/36 filled with water. (* only one echo evident)

To identify the path that causes each pattern, we compare the observed periods with the flight times calculated for the most likely paths through the system. We specifically consider the paths of through transmission, continuous circumferential propagation (around the cylinder wall), reflection from the liquid-loading interface and leaky paths that include conversion to bulk waves in the liquid. The paths of through transmission, circumferential propagation and reflection from the loading interface are show in Figure 4.6 (a) while Figure 4.6 (b), (c) and (d) show leaky paths. The nature of these paths are described next. Many of these paths were identified by Shannon *et al* [32].

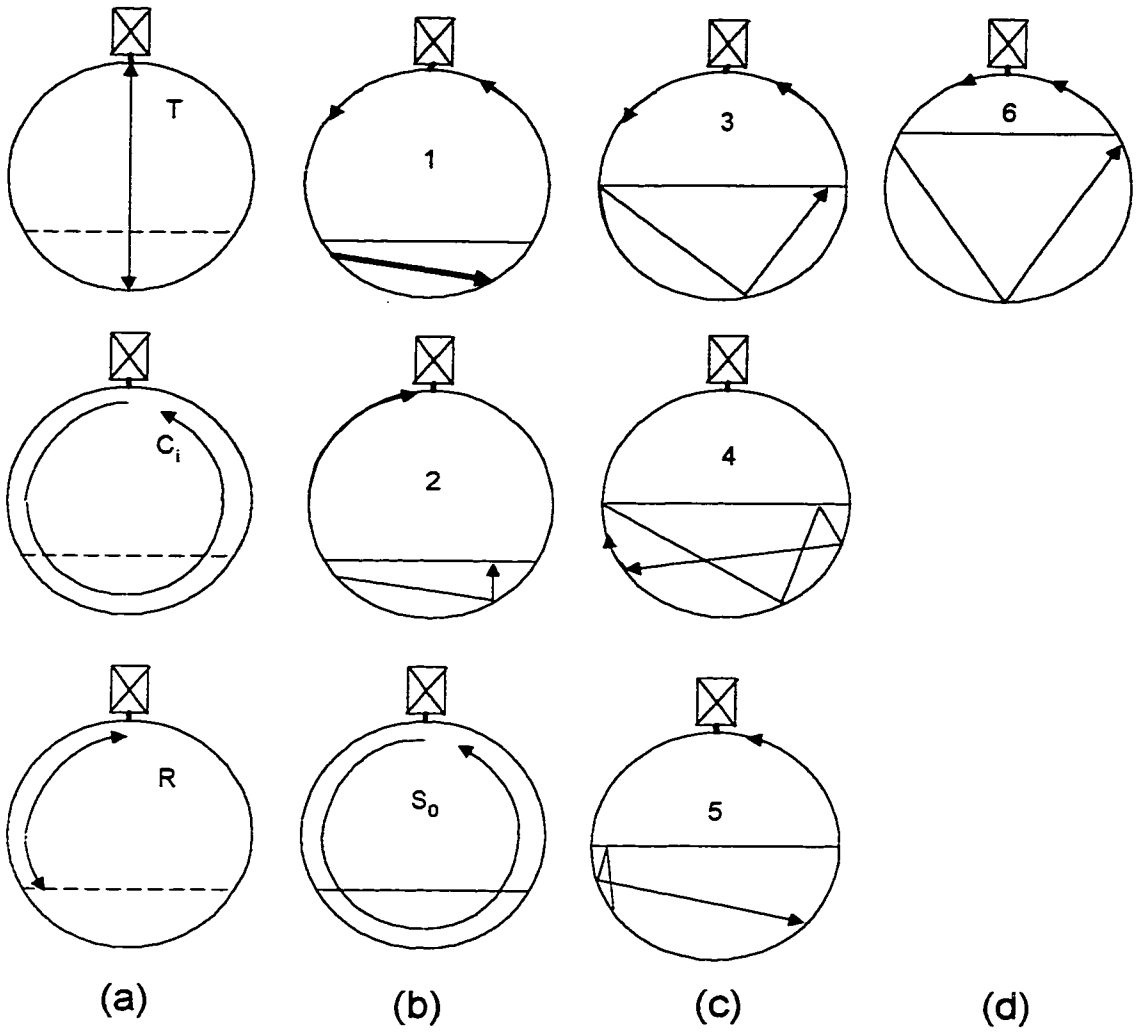

Figure 4.6 Illustration of paths through the water-loaded aluminum shell (a) paths in all levels: through transmission (T), circumferential (C_i) and reflected (R) paths, (b) ¼ filled shell, (c) ½ filled shell, (d) 2/3 filled shell.

Recall that "through transmission" refers to the direct acoustic path from the transducer straight down through the interior of the shell to its bottom wall, and directly back to the transducer. We calculate the time for this round trip at all fill levels.

"Circumferential propagation" refers to the circular propagation of an acoustic pulse along the shell wall. When considering circumferential propagation, we are not sure *a priori* whether the loaded portion of the shell primarily supports the A_0^L, S_0^L or a

coupled mode. We therefore calculate the flight times for these three cases. That is, we calculate the flight times for circumferential propagation of

(a) the A_0 and A_0^L modes in the unloaded and loaded portions of the shell, respectively. We refer to this case as the circumferential path C (A_0/A_0^L),

(b) the S_0 and S_0^L modes in the unloaded and loaded portions of the shell, respectively (circumferential path C (S_0/S_0^L)),

(c) the A_0 and coupled mode (circumferential path C (A_0, coupled).

The leaky paths are a little more complicated. Path 1 (shown in Figure 4.6), for example, begins as an A_0 mode that is produced in the unloaded shell continues down into the loaded portion of the shell as the A_0^L mode where it is converted (leaked) to a bulk wave in the liquid. After travelling through the water for some distance, the bulk wave is reconverted to the A_0^L mode in the shell, and returns to the transducer.

Path 2 is similar to path 1 up until where the leaked energy strikes the shell wall. In path 2, we follow the energy reflected from the wall. This reflected energy bounces off the water's surface and is directed back to the transducer along the path from which it came.

Paths 3, 4 and 5 share common path elements. Path 3 is similar to path 2 up until where it strikes the water surface. If we take beam width into consideration, we find that part of the energy in path 3 strikes the shell just below the liquid surface, where it is converted to an A_0^L wave and travels back to the transducer. The portion reflected by the liquid surface travels along path 4. Path 5 is the same as path 4 up until the point

where the bulk energy in path 4 is reconverted into the A_0^L mode in the shell. Path 5 tracks the energy reflected from this point onward.

The theoretical flight times for the paths shown in Figure 4.6 are listed in Table 4.2, where they are also compared to the experimental flight times. Table 4.2 clearly shows that none of the times for the through transmission or circumferential paths match the experimental periods, while the leaky paths match the experimental periods quite well.

Fill level	Path	Theoretical flight times (μs)	Experimental periods (μs)	% Difference
1/4	Through	424.0	-	-
	$C(A_0/A_0^L)$	93.5	-	-
	$C(S_0/S_0^L)$	55.9	56.1	0.36
	$C(A_0$/coupled)	110.12	-	-
	Reflected	62.4	-	-
	1	112.3	111.8 ± 1.1	0.40
	2	163.0	163.0 ± 0.3	0
1/2	Through	323.0	-	-
	$C(A_0/A_0^L)$	93.5	-	-
	$C(S_0/S_0^L)$	55.9	-	-
	$C(A_0$/coupled)	112.4	-	-
	Reflected	46.1	-	-
	3	132.9	130.5 ± 1.3	1.84
	4	192.4	197.5 ± 1.5	2.58
	5	86.6	84.1 ± 0.8	2.97
25/36	Through	245.0	-	-
	$C(A_0/A_0^L)$	93.5	-	-
	$C(S_0/S_0^L)$	55.9	-	-
	$C(A_0$/coupled)	114.1	-	-
	Reflected	34.5	-	-
	6	132.9	133.4 ± 0.5	0.37

Table 4.2 Flight times for the paths shown in Figure 4.6 compared to experimentally observed periods

The comparisons in Table 4.2 strongly suggest that acoustic energy travels along the paths 1 through 6. These paths all include leakage of the A_0^L mode into the liquid.

That the pulse travels for a stint as a bulk wave through the liquid was confirmed when objects were placed inside the liquid so as to bisect these paths; the signals from the obstructed shell were found to differ from the signals in the unobstructed shell.

4.2 Stainless steel shell

Pulse-echo experiments were performed on the stainless steel shell at fd = 0.64, 0.80, 0.96 MHz mm. Alternately, since a single stainless steel shell was tested, one can think of the experiments as being performed at three frequencies, f = 0.8, 1.0, 1.2 MHz.

The waveforms were found to differ significantly at different liquid heights, but not at different frequencies so that the waveforms acquired at ½ fill at 0.8 MHz and 1.0 MHz were very similar.

4.2.1 Empty shell group velocity

Figure 4.9 shows the waveform for the empty stainless steel shell at fd = 0.64 MHz mm. The waveforms in the empty shell at fd = 0.8 and 0.96 MHz mm are almost identical to the one shown in Figure 4.9. The echoes in Figure 4.9 are separated by 29.08 μs, corresponding to a group velocity of 3208.6 m/s around the circumference of the shell. This matches the theoretical value of group velocity for the A_0 mode shown in Figure 2.4. We can see that the amplitudes of the echoes do not decrease monotonically in time. It is thought that this modulation is caused by the edge effects of the (narrow) stainless steel shell.

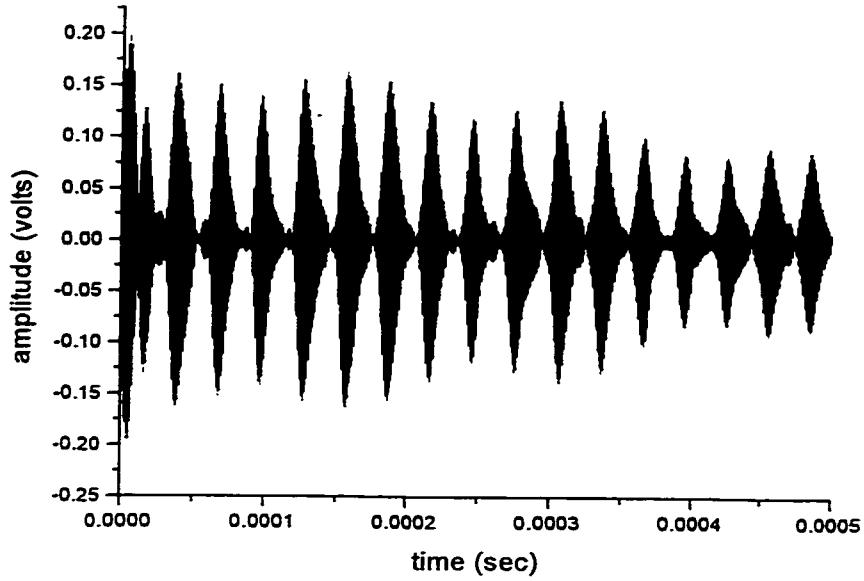

Figure 4.7 Waveform acquired at 0.8 MHz (fd = 0.64 MHz mm) from the empty stainless steel shell.

4.2.2 Empty shell phase velocity

The results for this experiment were similar to those for the aluminum shell in that the group velocity was inadvertently measured. Details of the experiment and analysis can be found in Appendix B.

4.2.3 Partially-filled shell

When the shell is partially filled with water, we observe a great myriad of echoes that, due to the small radius of the stainless steel shell, are closer together than the echoes observed in the aluminum shell. These echoes interfere with one another soon after the initial pulse, possibly amplifying minor echoes and removing significant echoes where

constructive and destructive interference, respectively, occurs. It is therefore difficult to piece together families of echoes as we did for the aluminum shell. Indeed, the simulation that worked somewhat well for the aluminum shell finds a limit to its applicability here.

One family of echoes does emerge, however, at each value of fd. The average periods for each family is listed in Table 4.3, along with the number of significant (large) echoes in the waveform contributing to the average period. Figure 4.12 shows the family when the shell is 7/18 full at 1.0 MHz (fd = 0.8 MHz mm).

Fill	0.64 MHz mm		0.8 MHz mm		0.96 MHz mm	
(x/18)	Period (μs)	# Echoes	Period (μs)	# Echoes	Period (μs)	# Echoes
0	30.04	16	28.91		-	0
2	-	0	32.73	4	-	0
3	-	0	30.15	5	-	0
4	35.59	5	32.51	8	-	0
5	36.61	5	-	0	-	0
6	36.91	6	35.85	13	-	0
7	36.82	6	35.97	11	-	0
8	37.62	13	35.86	5	35.20	9
9	37.34	17	35.75	9	-	0
10	37.19	6	36.18	9	34.47	11
11	37.86	13	35.93	6	34.18	9
12	37.53	17	36.23	7	35.45	3
13	38.79	12	36.06	11	-	0
14	36.91	6	36.85	9	-	0
15	43.40	4	40.42	4	35.51	4
16	43.40	4	40.42	4	-	0

Table 4.3 Observed periods for echoes at all water fill levels in the stainless steel shell for the three values of fd tested. The fill column refers to the proportion of the tube filled (e.g. 0/18 is empty and 9/18 is half full). Dash marks indicate that no echo patterns were found.

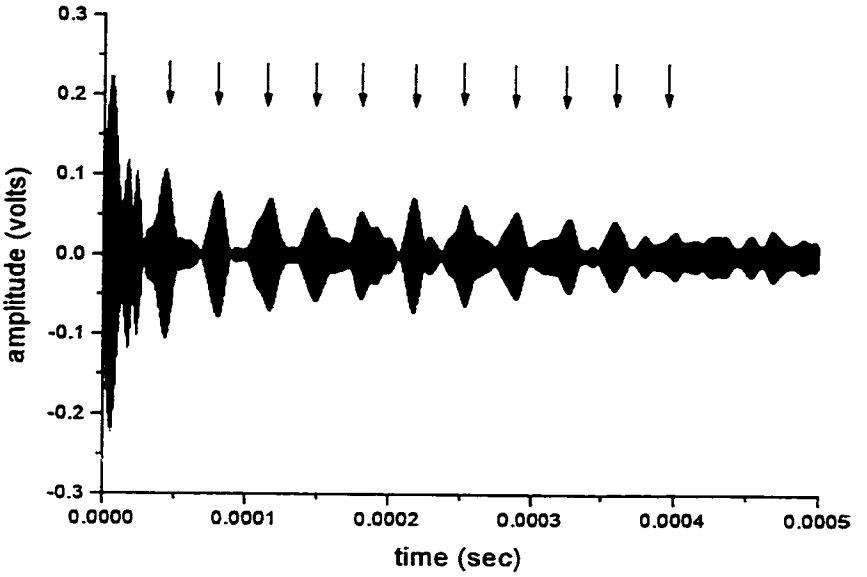

Figure 4.8 Waveform acquired with stainless steel shell 7/18 full of water at 1.0 MHz (fd = 0.8 MHz mm)

As we did for the aluminum shell, we compared the periods observed to the theoretical flight times for the paths of through transmission (T), circumferential (C) and leaky (L) waves at fd = 0.64, 0.8 and 0.96 MHz mm (Figure 4.12).

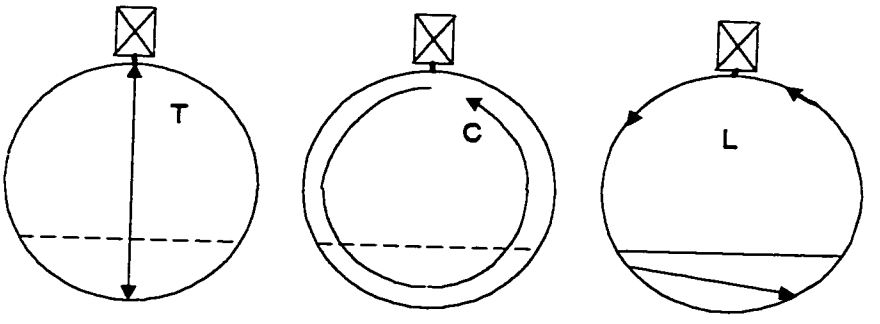

Figure 4.9 Through transmission (T), circumferential (C), and leaky (L) paths in the partially filled stainless steel shell.

The theoretical and observed flight times at fd = 0.64, 0.8 and 0.96 MHz mm are listed in Table 4.4. We can immediately see from Table 4.4 that the times for through transmission do not match the experimental times. The flight times for the other modes are graphed in Figures 4.13. Except for at fills 15/18 and 16/18 in Figure 4.13 (a) and (b), there is a very close match between the theoretical leaky times (curve 'L') and experiment.

Fill	T	C (A/A0L)	C (A0/coupled)	L	Experiment
4	71.1	29.4	32	36.1	32.5
5	67.5	29.4	32.4	36.1	
6	63.9	29.5	32.8	36.2	35.8
7	60.3	29.5	33.2	36.3	36
8	56.8	29.6	33.5	36.3	35.9
9	53.2	29.6	33.9	36.4	35.8
10	49.6	29.7	34.2	36.4	36.2
11	46	29.7	34.6	36.5	35.9
12	42.4	29.8	35	36.5	36.2
13	38.8	29.9	35.4	36.6	36.1
14	35.2	29.9	35.8	36.6	36.9
15	31.7	30	36.2	36.7	40.4
16	28.1	30.1	36.7	36.8	40.4

Table 4.4 Theoretical times of flight for pulses along the paths shown in Figure 4.12; T for the path of through transmission; C (A_0/A_0^L) for the A_0 & A_0^L modes around the cylinder wall; C (A_0/coupled) for the A_0 & coupled modes around the cylinder wall; L is the leaky path; 'Experiment' are the observed periods

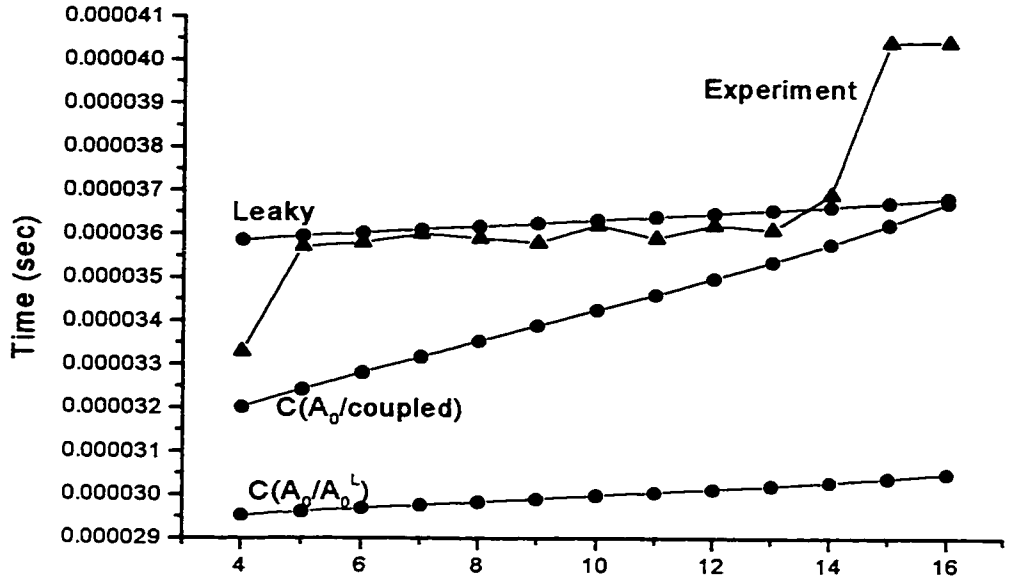

Figure 4.10 (a) Comparison of theoretical and experiment flight times at all fill levels in the stainless steel shell at fd = 0.64 MHz mm

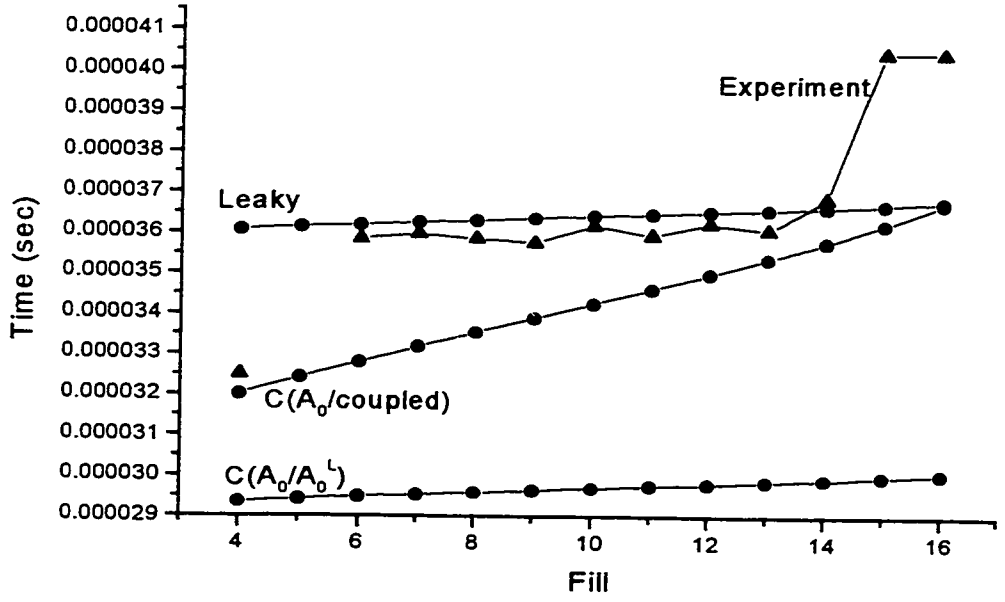

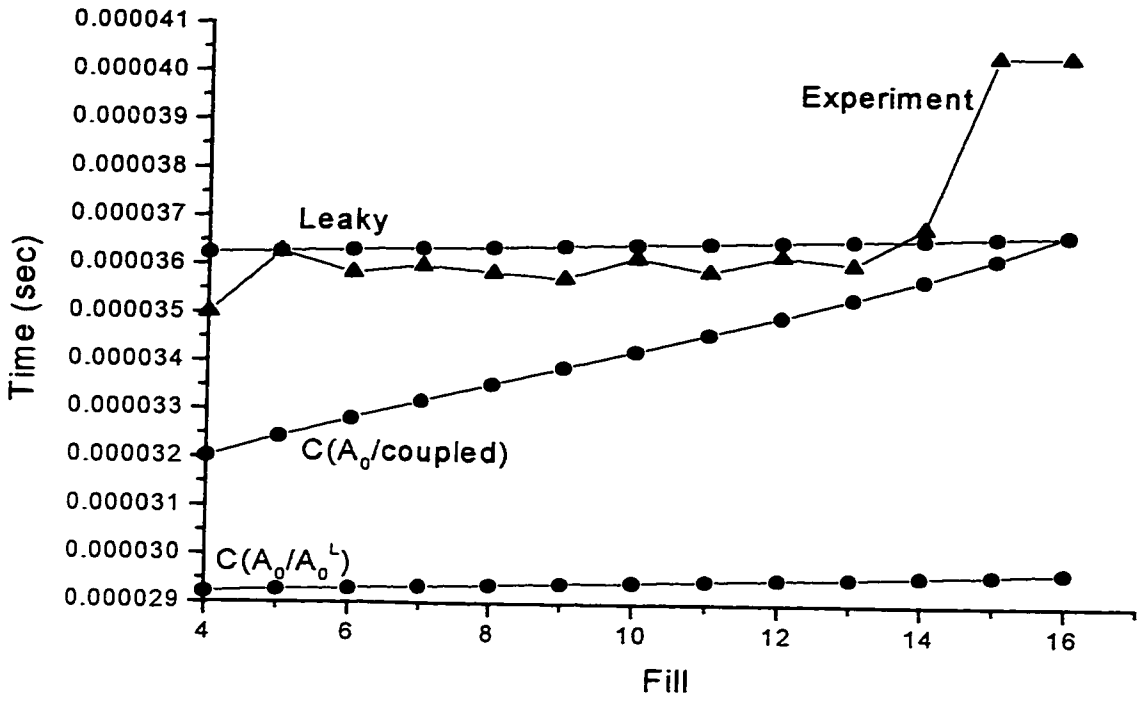

Figure 4.10 (b), (c) Comparison of theoretical and experiment flight times at all fill levels in the stainless steel shell at (b) fd = 0.8 MHz mm, (c) 0.96 MHz mm.

4.3 Discussion

We have the result that both the aluminum and the stainless steel shells seem to preferentially support the leaky A_0^L mode in the loaded portion of the shells. Why aren't the coupled modes supported? While an exact answer to this question is not given here, we note that it would seem reasonable for the A_0^L mode to be produced in the loaded portion of the shell since this mode is the natural continuation of the A_0 mode from the unloaded portion of the shell.

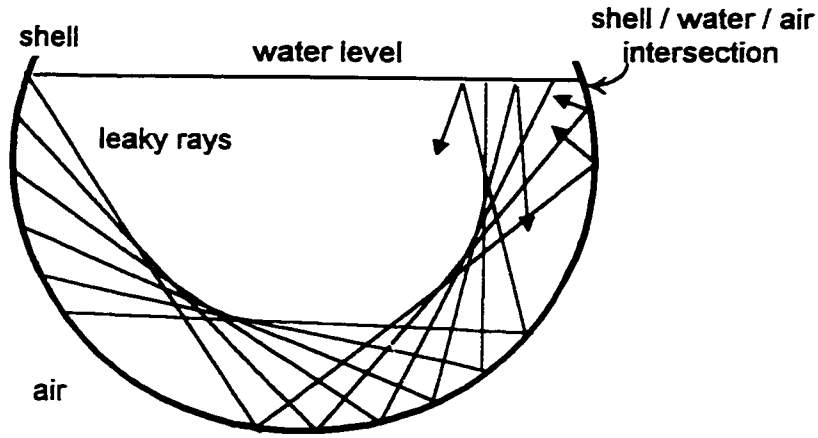

Figure 4.11 The splitting of the bulk wave in the liquid filler of the stainless steel shell.

Due to the rather messy nature of the echoes gathered from the stainless steel shell, we found that we could not use the simulation to successfully track the energy in the this shell. It is believed that this limitation results from the shell radius being comparable to the beam width in the stainless steel shell. Recall that stainless steel has a lower attenuation coefficient, so that the acoustic energy leaks from the A_0^L at a slower rate than it does in the aluminum shell. This causes the beam in the liquid to be wider (Figure 4.11). There is now more chance that the beam, after redirection with the shell wall, will be split by its encounter with the shell/liquid/air intersection. This splitting breaks a beam into two new beam that reflect off in different directions. The simulation's representation of the beam by a single ray is no longer valid in this case.

5. CONCLUSION

In this research, we have presented the theory of Lamb mode propagation, attenuation, leakage and particle displacement in free and liquid-loaded plates. We have reviewed the theory of reflection and transmission of a bounded beam at a the surface of a plate. We have analyzed the effects of transmission of the A_0 Lamb mode across a loading discontinuity, and considered its possible conversion to a coupled mode in the loaded portion of the shell.

Experimental work was performed to identify the paths taken by the acoustic energy through aluminum and stainless steel shells containing water. A simulation was written that successfully identified the path for 70% of the major echoes taken from the partially-filled aluminum shell.

The simulation was unsuccessful for the most part in identifying the source of the echoes in the stainless steel shell. It is hypothesized that the smaller dimension of this shell combined with the greater leaky distance for the A_0^L mode conspire to limit the applicability of the simulation's use of acoustic rays to represent bulk waves in the liquid. One major family was, however, identified in most of the waveforms acquired from the stainless steel shell. It was shown that the path associated with this family most likely includes leakage of the A_0^L mode into the water filler.

We have the experimental result that both the partially-filled aluminum and stainless steel shells support the A_0^L rather than a coupled mode along the liquid-loaded shell wall. This result seems reasonable given that the shell mode below the liquid surface is produced by an A_0 mode travelling down the shell wall across the loading boundary.

The stainless steel experiments would most likely yield better results if they were performed on larger shells. This would require a robust contact transducer that could withstand the increased input voltage that would be needed to receive a signal. Further work could also be done to improve the impedance match of the transducer coupling. Currently, the poor match of the thin line of couplant limits to the amount of energy that can safely be fed to the transducer.

The simulation was somewhat successful in predicting echo times in the aluminum shell. There will always be the limitation, however, that the acoustic beam formed in the liquid will be split in two, possibly causing additional echoes to appear at the transducer. The first improvement to the simulation would be to somehow account for beam width.

As for the feasibility of using circumferential modes for non-intrusive level sensing, there is no sweeping conclusion to this issue. Circumferential mode sensors have promise for relatively large thin-walled structures, where leaky distances are small compared to shell radii. Other shells would be ill-suited to this type of sensing either because of their small attenuation or difficult geometry.

REFERENCES

1. Liu, Y., and L.C. Lynnworth, "Flexural Wave Sidewall Sensor for Noninvasive Measurement of Dicrete Liquid Levels in Large Storage Tanks," *IEEE Ultrasonics Symposium*, 385-388, 1993

2. Cheeke, J.D.N., X. Li, Z. Wang, "Characteristics of circumferential waves in thin walled tube acoustic devices", 1995 IEEE Ultrasonics Symposium

3. Li, X., J.D.N. Cheeke, Z. Wang, Jen C.K., M. Viens, G. Yi, and M. Sayer, "Ultrasonic Thin-Walled Tube Wave Devices for Sensor Applications," *Appl. Phys. Lett.*, 67 (1), 37-39, 3 July 1995

4. Li, X., Z. Wang, C.-K. Jen, M. Viens, J. D. N Cheeke, "Ultrasonic thin-walled tube wave structures for sensing devices", IEEE Transactions on Ultrasonics, Ferroelectrics and Frequency Control, 43 (2), 1-6, March 1996

5. Veksler, N. D., J.-L. Izbicki, J.-M. Conoir, "Flexural waves in the acoustic wave scattering by a liquid-filled shell", Acoustical Physics, 45 (3), 279-288, 1999

6. G. Maze, private communication, January 1999

7. X. Li, doctoral dissertation, Concordia University, 2000

8. Ahyi, A.C., P. Pernod, and O. Gatti, "Experimental Demonstration of the Pseudo-Rayleigh (A0) Wave," *J. Acoust. Soc. Am.*, 104 (5), 2727-2732, Nov. 1998

9. Choi, M.S., M.S. Yang, and H.C. Kim, "Detection of Leak-Defective Fuel Rods Using the Circumferential Lamb Waves Excited by the Resonance Backscattering of Ultrasonic Pulses," *Ultrasonics*, Vol 30, No 4, 221-223, 1992

10. Veksler, N.D., J.L. Izbicki, and J.M. Conoir, "Bending A Wave in the Scattering by a Circular Cylindrical Shell: Its Relation with Free Modes," *J. Acoust. Soc. Am.*, 96 (1), 287-293, July 1994

11. Maze, G., Léon F., and Ripoche J., "Nature de l'Onde d'Interface de Scholte Sur Une Coque Cylindrique," *Acustica*, 81, 1995, 201-213

12. H. Lamb, "On waves in an elastic plate" Proc. Roy. Soc. London A 93, 114,1917

13. Osborne, M.F.M., and S.D. Hart, "Transmission, Reflection and Guiding of an Exponential Pulse by a Steel Plate in Water. I. Theory," *J. Acoust. Soc. Am.*, 17 (1), 1-18, July 1945

14. Grabowska, A., "Propagation of Elastic Wave in Solid Layer-Liquid System," *Archives of Acoustics*, 4, 1, 57-64, 1979

15. Talmant, M., "Rétrodiffusion d'une impulsion ultrasonore brève par une coque

cylindrique à paroi mince", Ph.D. thesis, University of Paris VII, 1987

16. Victorov, I. A, Rayleigh and Lamb waves, Plenum Press, New York, 1967

17. Deighton, M.O., A.B. Gillespie, R.B. Pike, and R.D. Watkins, "Mode Conversion of Rayleigh and Lamb Waves to Compression Waves at a Metal-Liquid Interface," *Ultrasonics*, 249-258, Nov. 1981

18. Talmant, M., Quentin G., J.L. Rousselot, J.V. Subrahmanyam, and H. Überall, "Acoustic Resonances of Thin Cylindrical Shells and the Resonance Scattering Theory," *J. Acoust. Soc. Am.*, 84 (2), 681-688, Acoustical Society of America, August 1988

19. Dragonette, L. R., "Schlieren Visualization of Radiation Caused by Illumination of Plates with Short Acoustical Pulses," *J. Acoust. Soc. Am.*, 51 (3), pt. 2, 920-935, 1972

20. Dabirikhah, H., C. W. Turner, "Anomalous behaviour of flexural waves in very thin immersed plates", 1992 IEEE Ultrasonics Symposium, 313-317, 1992

21. Brekhovskikh, L. M., Waves in Layered Media, Academic Press, New York, 1980

22. Chimenti, D. E., S. I. Rokhlin, "Relationship between leaky Lamb modes and reflection coefficient zeroes for a fluid-coupled elastic layer", *J. Acoust. Soc. Am.*, 88 (3), 1603-1611, 1990

23. Mott, G., "Reflection and refraction coefficients at a fluid-solid interface", *J. Acoust. Soc. Am.*, 50 (3), Pt. 2, 819-829, November 1970

24. Schoch, A., *Acustica* 2, 18-19, 1952

25. Feit, D., Y. N. Liu, "The nearfield response of a line-driven fluid-loaded plate", *J. Acoust. Soc. Am.*, 78 (2), 763-766, August 1985

26. Matula, T.J., and P.L. Marston, "Energy Branching of a Subsonic Flexural Wave on a Plate at an Air-Water Interface. I. Observation of the Wave Field Near the Interface and Near the Plate," *J. Acous. Soc. Am.*, 977 (3), 1389-1398, *Acoustical Society of America*, March 1995

27. Lord Rayleigh, "On the free vibrations of an infinite plate of homogenous isotropic elastic matter, *Proc. Lond. Math. Soc.* 20, 225, 1889

28. Maze G., Cheeke, J.D.N., X. Li, Z. Wang, "Interface acoustic modes in water-filled thin-walled cylindrical shells", submitted to *J. Acoust. Soc. Am.* August 2000

29. Cheeke, J.D.N., X. Li, Z. Wang, "Observation of flexural lamb waves (A_0 mode) on water-filled cylindrical shells", *J. Acoust. Soc. Am.* 104 (6), 3678-3680, December 1998

30. Talmant, M., H. Uberall, R.D. Miller, M.F. Werby, and J.W. Dickey, "Lamb Waves

and Fluid-Borne Waves on Water-Loaded, Air-Filled Thin Spherical Shells," *J. Acoust. Soc. Am.*, 86 (1), 278-289, Acoustical Society of America, July 1989

31. Krautkrämer, J., H. Krautkrämer, Ultrasonic testing of materials, 4th edition, Springer-Verlag, Berlin, 1990

32. Shannon, K., Li. X, Z. Wang, and J.D.N. Cheeke, "Mode Conversion and the Path of Acoustic Energy in a Partially Water-Filled Aluminum Tube," *Ultrasonics*, 37, 303-307, 1999

APPENDIX A

A.1 Characteristic equations for fluid-loaded plate

Here we derive the characteristic equation for a plate that is fully immersed in a liquid, and a plate that that is in contact with a liquid on one surface and with air on the other (Eqn. 2.11). The symbols in this appendix are the same as those used in the text.

We start with a plate immersed in liquid. We have $\rho_1 = \rho_2$ and $v_1 = v_2$, so that $f_1 = -e_1$ and $f_2 = e_2$. Equation 2.7 becomes

$$HA = \begin{bmatrix} a_1 & b_1 & c_1 & d_1 & e_1 & 0 \\ -a_1 & b_1 & c_1 & -d_1 & 0 & -e_1 \\ a_2 & b_2 & c_2 & d_2 & e_2 & 0 \\ a_2 & -b_2 & -c_2 & d_2 & 0 & e_2 \\ a_3 & b_3 & c_3 & d_3 & 0 & 0 \\ -a_3 & b_3 & c_3 & -d_3 & 0 & 0 \end{bmatrix} \begin{bmatrix} A \\ B \\ C \\ D \\ E \\ F \end{bmatrix} = \begin{bmatrix} a_1 & d_1 & e_1 & 0 & 0 & 0 \\ a_2 & d_2 & e_2 & 0 & 0 & 0 \\ a_3 & d_3 & 0 & 0 & 0 & 0 \\ 0 & 0 & 0 & b_1 & c_1 & e_1 \\ 0 & 0 & 0 & b_2 & c_2 & e_2 \\ 0 & 0 & 0 & b_3 & c_3 & 0 \end{bmatrix} \begin{bmatrix} A \\ B \\ C \\ D \\ E \\ F \end{bmatrix} = 0$$

(Eqn. A.1)

Solutions to Equation A.1 exist when $|H| = 0$, i.e, when

$$|H| = |H_{SF}||H_{AF}| = 0 \text{ where} \qquad \text{(Eqn. A.2)}$$

$$|H_{SF}| = \begin{vmatrix} a_1 & d_1 & e_1 \\ a_2 & d_2 & e_2 \\ a_3 & d_3 & 0 \end{vmatrix} = \begin{vmatrix} a_2 & d_2 \\ a_3 & d_3 \end{vmatrix} - \frac{e_2}{e_1} \begin{vmatrix} a_1 & d_1 \\ a_3 & d_3 \end{vmatrix} = |H_S| - L_{SF} = 0$$

$$|H_{AF}| = \begin{vmatrix} b_1 & c_1 & e_1 \\ b_2 & c_2 & e_2 \\ b_3 & c_3 & 0 \end{vmatrix} = \begin{vmatrix} b_2 & c_2 \\ b_3 & c_3 \end{vmatrix} - \frac{e_2}{e_1} \begin{vmatrix} b_1 & c_1 \\ b_3 & c_3 \end{vmatrix} = |H_A| - L_{AF} = 0$$

These lead to the characteristic equations for the symmetric and antisymmetric modes in a plate immersed in a liquid:

$$(R_T^2 + k^2)^2 \tanh(R_T e) - 4k^2 R_T R_L \tanh(R_L e) - \frac{\rho_1 R_L}{\rho R_L} k^4 \sinh(R_L e) \sinh(R_T e) = 0$$

(Eqn. A.3 a)

$$(R_T^2 + k^2)^2 \coth(R_T e) - 4k^2 R_T R_L \coth(R_L e) - \frac{\rho_1 R_L}{\rho R_L} k^4 \cosh(R_L e) \cosh(R_T e) = 0$$

(Eqn. A.3 b)

A plate that is in contact with water on one surface and with air (vacuum) on the other has the five boundary conditions

(a) $u_z = (u_z)_1$ at z = e/2,

(b) $p_{xz} = 0$ at z = e/2,

(c) $p_{xz} = 0$ at z = -e/2

(d) $p_{zz} = 0$ at z = e/2,

(e) $p_{zz} = 0$ at z = -e/2,

(Eqn. A.4)

We have that $|H(\rho_2 = 0)| = 0$. Equation 2.7 becomes

$$|H(\rho_2 = 0)| = \begin{vmatrix} a_1 & b_1 & c_1 & d_1 & e_1 \\ -a_2 & b_2 & c_2 & -d_2 & 0 \\ a_2 & -b_2 & -c_2 & d_2 & e_2 \\ a_3 & b_3 & c_3 & d_3 & 0 \\ -a_3 & b_3 & c_3 & d_3 & 0 \end{vmatrix} = \begin{vmatrix} a_1 & d_1 & e_1 & b_1 & c_1 \\ a_2 & d_2 & e_2/2 & 0 & 0 \\ a_3 & d_3 & 0 & 0 & 0 \\ 0 & 0 & -e_2/2 & b_2 & c_2 \\ 0 & 0 & 0 & b_3 & c_3 \end{vmatrix} \quad \text{(Eqn. A.5)}$$

$$= e_1 \begin{vmatrix} a_2 & d_2 \\ a_3 & d_3 \end{vmatrix} \begin{vmatrix} b_2 & c_2 \\ b_3 & c_3 \end{vmatrix} - \frac{e_2}{2}\left(a_1 d_3 \begin{vmatrix} b_2 & c_2 \\ b_3 & c_3 \end{vmatrix} - a_3 d_1 \begin{vmatrix} b_2 & c_2 \\ b_3 & c_3 \end{vmatrix} \right) - \frac{e_2}{2}\left(a_2 d_3 \begin{vmatrix} b_1 & c_1 \\ b_3 & c_3 \end{vmatrix} - a_3 d_2 \begin{vmatrix} b_1 & c_1 \\ b_3 & c_3 \end{vmatrix} \right)$$

$$= e_1 \begin{vmatrix} a_2 & d_2 \\ a_3 & d_3 \end{vmatrix} \begin{vmatrix} b_2 & c_2 \\ b_3 & c_3 \end{vmatrix} - \frac{e_2}{2} \begin{vmatrix} b_2 & c_2 \\ b_3 & c_3 \end{vmatrix} \begin{vmatrix} a_1 & d_1 \\ a_3 & d_3 \end{vmatrix} + \frac{e_2}{2} \begin{vmatrix} b_1 & c_1 \\ b_3 & c_3 \end{vmatrix} \begin{vmatrix} a_2 & d_2 \\ a_3 & d_3 \end{vmatrix}$$

So,

$$\frac{|H(\rho_2 = 0)|}{e_1} = |H_S||H_A| - |H_S|\frac{L_{AF}}{2} - |H_A|\frac{L_{SF}}{2} = \left(|H_S| - \frac{L_{SF}}{2}\right)\left(|H_A| - \frac{L_{AF}}{2}\right) - \frac{L_{SF}L_{AF}}{4} = 0$$

(Eqn. A.6)

And the characteristic equation becomes

$$\left(|H_S| - \frac{L_{SF}}{2}\right)\left(|H_A| - \frac{L_{AF}}{2}\right) - \frac{L_{SF}L_{AF}}{4} = 0 \qquad \text{(Eqn. A.7)}$$

A.2 Particle displacements

We derive the particle motions for the symmetric modes and antisymmetric modes next. For brevity, we have omitted the factor $e^{i\omega t}$ from the expressions below. The variables A to F can be determined by simple substitutions in the matrix of Equation A.1 for the plate in vacuum or Equation A.5 for the plate with one side water loading. In particular, we have,

$$A = \frac{-(R_T^2 + k^2)\sinh(R_T e)}{2ikR_L \sin g(R_L e)} D,\ B = \frac{-(R_T^2 + k^2)\cosh(R_T e)}{2ikR_L \cosh(R_L e)} C, \text{ and} \qquad \text{(Eqn. A.8)}$$

$$E = \frac{k_T^2 e^{R_1 d}}{2ikR_L}\left(D\sinh(R_T d) + C\cosh(R_T d)\right).$$

Symmetric mode: We have $\varphi = A\cosh(R_L z)e^{ikx}$, $\Psi = D\sinh(R_T z)e^{ikx}$, and

$$u_{XS}(x,z,D) = \frac{\partial\varphi}{\partial x} + \frac{\partial\Psi}{\partial z} = Aik\cosh(R_L z) + DR_T\cosh(R_T z) \qquad \text{(Eqn. A.9 a)}$$

$$= D\left[\frac{-(R_T^2 + k^2)\sinh(R_T e)}{2RL\sinh(R_L e)}\cosh(R_L z) + R_T\cosh(R_T z)\right]e^{ikx}$$

$$u_{ZS}(x,z,D) = \frac{\partial\varphi}{\partial z} - \frac{\partial\Psi}{\partial x} = AR_L\sinh(R_L z) - Dik\sinh(R_T z) \qquad \text{(Eqn. A.9 b)}$$

$$= D\left[\frac{i(R_T^2 + k^2)\sinh(R_T e)}{2k\sinh(R_L e)}\sinh(R_T z) - ik\sinh(R_T z)\right]e^{ikx}$$

$$u_{1XS}(x,z,D) = \frac{\partial\phi_1}{\partial x} = ikEe^{-R_1 z}e^{ikx} = D\frac{k_T^2}{2R_1}e^{R_1(d-z)}e^{ikx}\sinh(R_T d) \qquad \text{(Eqn. A.9 c)}$$

$$u_{1ZS}(x,z,D) = \frac{\partial\phi_1}{\partial z} = -R_1 Ee^{-R_1 z}e^{ikx} = D\frac{ik_T^2}{2k}e^{R_1(d-z)}e^{ikx}\sinh(R_T d) \qquad \text{(Eqn. A.9 d)}$$

Antisymmetric mode: We have $\varphi = B\sinh(R_L z)e^{ikx}$, $\Psi = C\cosh(R_T z)e^{ikx}$, and

$$u_{XA}(x,z,C) = \frac{\partial\varphi}{\partial x} + \frac{\partial\Psi}{\partial z} = Bik\sinh(R_L z) + CR_T\sinh(R_T z) \qquad \text{(Eqn. A.10 a)}$$

$$= C\left[\frac{-(R_T^2 + k^2)\cosh(R_T e)}{2R_L\cosh(R_L e)}\sinh(R_L z) + R_T\sinh(R_T z)\right]e^{ikx}$$

$$u_{ZA}(x,z,C) = \frac{\partial\varphi}{\partial z} - \frac{\partial\Psi}{\partial x} = BR_L\cosh(R_L z) - Cik\cosh(R_T z) \qquad \text{(Eqn. A.10 b)}$$

$$= C\left[\frac{i(R_T^2 + k^2)\cosh(R_T e)}{2k\cosh(R_L e)}\cosh(R_L z) - ik\cosh(R_T z)\right]e^{ikx}$$

$$u_{1XA}(x,z,D) = \frac{\partial\phi_1}{\partial x} = ikEe^{-R_1 z}e^{ikx} = C\frac{k_T^2}{2R_1}e^{R_1(d-z)}e^{ikx}\cosh(R_T d) \qquad \text{(Eqn. A.10 c)}$$

$$u_{1ZS}(x,z,D) = \frac{\partial\phi_1}{\partial z} = -R_1 Ee^{-R_1 z}e^{ikx} = C\frac{ik_T^2}{2k}e^{R_1(d-z)}e^{ikx}\cosh(R_T d) \qquad \text{(Eqn. A.10 d)}$$

The variables C and D serve as the amplitude of the two waves. In the equation for u_z we can see that the A and D terms in equation A.9 (b) both have hyperbolic cosine factors. These odd factors account for the symmetric mode's equal and opposite displacement u_z across the z = 0 plane, i.e. for its symmetric nature. The B and C terms of u_z in Equation A.10 (b) have (even) hyperbolic sine factors, which are antisymmetric with respect to z = 0.

APPENDIX B

This appendix describes the results of the phase velocity experiments that were performed on an aluminum shell and the stainless steel shell.

For technical reasons, the aluminum shell tested in the phase velocity experiment was not the same as the one tested in the partial-fill experiments described in the main body of this thesis. The aluminum shell here had an outer radius of 1" (25.4 mm) and a wall thickness of 0.28" (0.71 mm).

The experiment itself was outlined in Section 3.4. Below are specific parameters used in the experiment on the aluminum shell

Repetition rate	= 500 Hz
Time between input pulses	= 2 ms
Pulse length	= 90 μs (kept constant at all frequencies)
Time for circumference of a pulse	= 49.9 μs

Figure B.1 illustrates key periods in a typical waveform. The horizontal lines at the top of the figure indicate the periods for the arrival of the input pulse after having circumnavigated the shell 'x' number of times (e.g. '3rd c.' refers to the reception of the third circumnavigation). Notice that each line is 90 μs long and one line starts every 49.9 μs. Again, this means that every circumnavigation lasts for 90 μs and it takes 49.9 μs for the leading edge of the pulse to reappear at the transducer. Notice that consecutive lines overlap (i.e. interfere with) one another in the regions marked 'int' at

the bottom of the figure.

The signal was acquired between 90 μs and 290 μs. The delay of 90 μs was set so that we could inspect more of the overlapping (later) portion of the signal.

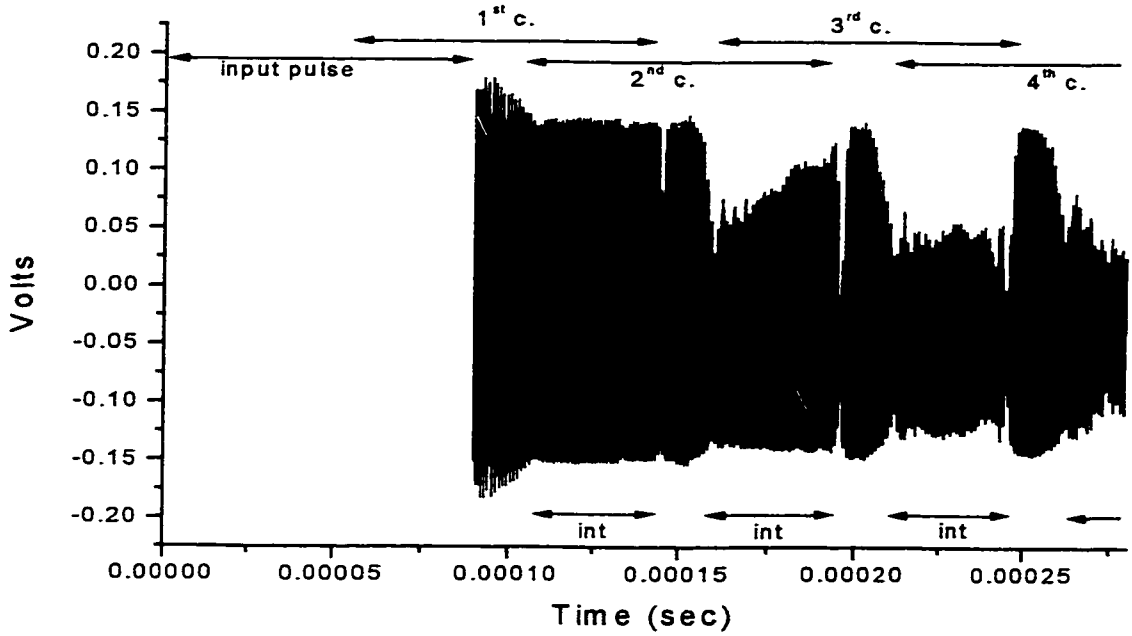

Figure B.1 Waveform from phase velocity experiment taken at f = 0.95 MHz

As the frequency is varied, the wavelength of the pulse is varied proportional to this frequency variation, and the two waves in an 'int' region interfere with one another in a constructive or destructive manner. A measure of this interference is given in the average amplitude of the rectified signal.

Figure B.2 shows the average rectified signal at various frequencies close to 1 MHz. The average frequency difference, Δf_{min}, between the local minima in this figure is

0.020 MHz. According to Equation 3.1

$$v_p = 2\pi r \Delta f_{min} \qquad \text{(Eqn. 3.1)}$$

Δf_{min} corresponds to a phase velocity of 3191.9 m/s. This value is almost perfectly equal to the group velocity for aluminum at the fd = 1 MHz x 0.7 mm = 0.7 MHz mm. The phase velocity is equal to 1900 m/s at this point on the dispersion curve.

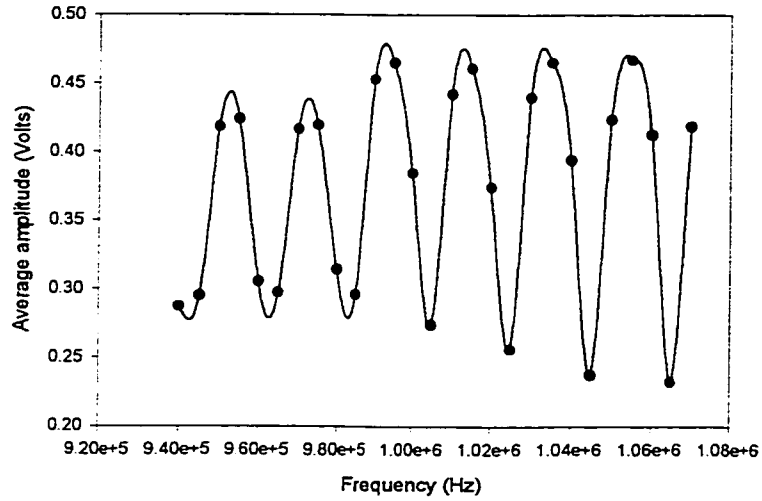

Figure B.2 Average amplitude vs. frequency around 1.0 MHz in empty aluminum shell

Figure B.3 shows the results of the phase velocity experiment at fd = 0.64 MHz mm on the empty stainless steel shell. The average separation, Δf_{min}, between the local minima in this figure is 0.016 MHz. According to Equation. 3.1, Δf_{min} corresponds to a phase velocity of 3066 m/s. Like the experiment on aluminum, this value is much closer to the group velocity than it is the phase velocity.

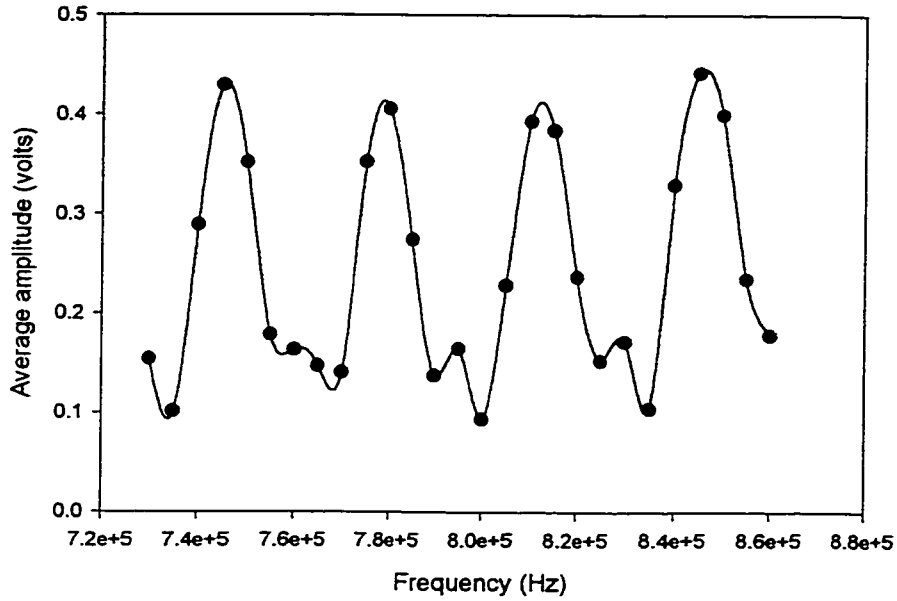

Figure B.3 Average amplitude vs. frequency around 0.8 MHz (fd = 0.64 MHz mm) in empty stainless steel shell